Extracellular vesicles Transfer Polarized Mitochondria and Increase Cellular Energetics in Ischemic Endothelial Cells

Anisha D'Souza[a], Amelia Burch[b], Wanzhu Zhao[a], Kandarp M. Dave[a], Courtney Sabatelle[a], Gina Joy[a], Nidia Quillinan[b], Paco S. Herson[b], and Devika S Manickam[a*]

[a]Graduate School of Pharmaceutical Sciences and School of Pharmacy, Duquesne University, Pittsburgh, PA, USA.

[b]Department of Anesthesiology, School of Medicine, University of Colorado Anschutz Medical Campus, Aurora, CO, USA.

***Corresponding author:**

Devika S Manickam, Ph.D.

453 Mellon Hall, 600 Forbes Avenue,

Pittsburgh, PA 15282.

Email: soundaramanickd@duq.edu, Twitter: @manickam_lab

Phone: +1 (412) 396-4722, Fax +1 (412) 396-2501

Running headline: EVs Transfer Polarized Mitochondria and Increase Cellular Energetics

Keywords

Extracellular vesicles, Mitochondrial transfer, ATP5A, Blood-Brain Barrier, Ischemic stroke, Endothelial protection

Abstract

Extracellular vesicles (EVs) such as exosomes (EXOs) and microvesicles (MVs) are promising carriers for the delivery of biologic drugs such as nucleic acids and proteins. We have demonstrated, *for the first time*, that EVs derived from hCMEC/D3: a human brain endothelial cell (BEC) line transfer polarized mitochondria to recipient BECs in culture and to neurons in mice acute brain cortical and hippocampal slices. This mitochondrial transfer increased ATP levels by 100 to 200-fold (relative to untreated cells) in the recipient BECs exposed to oxygen-glucose deprivation, an *in vitro* model of cerebral ischemia. Our previous studies suggested that EXOs, the smaller vesicle subpopulation, derived from a macrophage cell line (RAW264.7) load more exogenous plasmid DNA compared to the larger MVs and the RAW-derived EXOs also demonstrated greater transfection in the recipient BECs compared to EXOs derived from the homotypic hCMEC/D3 BECs. Proteomic analysis of EVs indicated that RAW-EVs are preferentially enriched with proteins that are involved in the trafficking of DNA-containing particles from the cytoplasm towards the nucleus. Intriguingly, although the heterotypic macrophage-derived EVs demonstrated increased transfection in the recipient BECs; the homotypic, BEC-derived EVs demonstrated a greater selectivity to transfer polarized mitochondria and increase endothelial cell survival under ischemic conditions.

Highlights

- EVs transfer polarized mitochondria to endothelial cells and acute brain slices
- Mitochondrial transfer increased ATP in ischemic brain endothelial cells (BECs)
- BEC-EVs demonstrate greater mitochondrial transfer to recipient BECs
- Macrophage-derived EVs are better DNA transfection agents in recipient BECs
- Macrophage-EVs are enriched in proteins associated with nuclear trafficking of DNA

1. Introduction

Ischemic stroke is the second leading cause of death worldwide. About 87% of all strokes are ischemic with one person dying every four minutes in the United States. The severe lack of therapeutic options [1, 2] other than tissue plasminogen activator (tPA), a viable option for only 5% of the patient population, is an urgent yet unmet clinical need. In ischemic stroke, the blood-brain barrier (BBB) is disrupted because of alterations to the endothelial tight junctions such as the phosphorylation of zona occludens, occludin, and claudin-5 and uncontrolled polymerization of endothelial cell actin resulting in the formation of F-actin-enriched stress fibers. Redistribution of junctional proteins results in paracellular leakiness increasing the permeation of macromolecules, infiltration of immune cells like macrophages, dendritic cells, and lymphocytes with the release of pro-inflammatory mediators like cytokines and chemokines [3]. These pathological processes exacerbate the overall injury leading to permanent neurovascular dysfunction and poor neurological outcomes. Depleted oxygen and nutrient supply decrease the overall cellular energy (ATP) levels and further generate reactive oxygen species resulting in mitochondrial dysfunction, decreased cell viability and trigger apoptotic endothelial and neuronal death [4, 5].

Although the traditional stroke pharmacotherapies singularly focused on neuroprotection, the emerging consensus points at the need to protect the cerebral microvasculature/BBB in addition to other cell types of the neurovascular unit [6-10]. Cerebral endothelial and neuronal cells respond equally rapidly to ischemic injury [11]. Functional damage of the BBB thus amplifies the neuronal damage and exacerbates potential cerebral hemorrhage. The brain endothelial cells (BECs) lining the BBB produce neuroprotectants like brain-derived neurotrophic factor (BDNF) at concentrations nearly 50*x* greater than that of cortical neurons [11]. Apart from that, the BBB also serves as an important production machinery for molecules such as metalloproteinases, platelet-derived growth factor, interleukins, fibronectin, endothelin that are required for neuronal nourishment and regulation of the vasomotor activities [12]. A functionally healthy endothelium can promote neurogenesis and neuronal recovery through matrix-trophic interactions [13]. In an elegant study using transgenic mice, Shi *et al.* demonstrated that endothelial- but *not* neuronal-expression of heat shock protein 27 (HSP27) protected the BBB integrity, decreased the infarct volumes, and also improved functional outcomes for as long as up to 28 days-post stroke in a mouse model of ischemic stroke. These effects were specifically attributed to the HSP27-mediated inhibition of actin polymerization in the BECs leading to effective suppression of its structural changes and the resulting effects on overall tight junction integrity post-stroke [14]. In summary, non-neuronal targeting of drugs in stroke will mitigate neuronal degeneration and enhance the repair processes [13]. Given the central role of the BECs in homeostatic and endothelial—neuronal matrix coupling-trophic signalling processes [11], we propose that targeting protection of the brain endothelial cells or the BBB itself in such cases will be an important component of stroke therapy [4].

The documented roles of cell-secreted extracellular vesicles (EVs) in intercellular communication via the transfer of their innate cargo make them attractive drug delivery carriers [15-19]. The natural origin of EVs may result in a lower immunogenicity and their increased stability in systemic circulation [20-23] makes them viable candidates for the delivery of biologics like nucleic acids and proteins. They can also traverse biological barriers including the blood-brain barrier [24] and have demonstrated cell-specific targeted delivery [4]. The host-derived "self" EVs can evade the host immune system by preventing unwanted phagocytosis and exhibit low immunogenicity in comparison to synthetic nanocarriers [4, 25]. The subtypes of EVs vary in particle diameters, amongst other factors. The larger, 100-1000 nm microvesicles (MVs), and the smaller, 50 – 150 nm exosomes (EXOs) are secreted via different biogenesis pathways [15, 26-29]. These EVs can also be engineered to be packaged with nucleic acids for gene therapy or gene silencing effects [4]. A few papers have reported plasmid DNA loading in EVs [30-32]. Kanada *et al.* loaded plasmid DNA [30] and minicircle DNA [33] in EVs. They reported that MVs were a better carrier for pDNA as the EXOs failed to show the gene expression in the recipient HEK293 cells [30]. Lamichhane *et al.* also loaded DNA into EVs via electroporation and found that the loading efficiency of DNA constructs are dependent upon the size of DNA. Plasmid DNA and linear DNA greater than 1000 bp could not be loaded in EVs with a reported upper loading limit of 5 μg of linear 250 bp dsDNA. Nevertheless, the loading efficiency of DNA was limited at 0.2 %, with poor transfection outcomes [31].

We speculated that brain endothelial cell-derived EVs may express a natural affinity to brain endothelial cells and therefore we engineered EVs derived from hCMEC/D3, a human brain

endothelial cell line, for the delivery of a model plasmid DNA. Following an ischemic insult, the inflammatory response to injury is triggered by the infiltration of peripheral immune cells through the disrupted endothelial junctions. Therefore, we also tested EVs derived from a macrophage cell line, RAW 264.7, as a delivery carrier. In our previous study, we have demonstrated that macrophage-derived EVs demonstrated increased luciferase transgene expression in the recipient brain endothelial cells (BECs) compared to the homotypic EVs isolated from brain endothelial cells and more interestingly, the smaller EV fraction, EXOs showed a greater DNA loading and transfection in the recipient BECs compared to the larger MVs [32]. The above results on EXO vs. MV-mediated DNA transfection were in direct contrast to previous observations reported by Kanada *et al*. [30] albeit their study used a different cell line, HEK293. To rule out operator-induced systematic biases in the transfection of the parent BECs using pDNA, isolation of DNA-loaded EVs and transfection of the recipient cells, we repeated the studies to confirm the DNA delivery potential of BEC- vs. macrophage-derived EVs. Our results were largely consistent with our previous study [32] and in this study, we conducted EV proteomic analyses to understand the reason behind the greater transfection of macrophage-derived exosomes.

The presence of a rich, innate biomolecular cargo in EVs can be exploited for additive/synergistic therapeutic effects depending on the drug cargo that is packaged in these vesicles. Specifically, EVs are reported to contain mitochondria, mitochondrial proteins, or mitochondrial DNA that can be transferred from the parent/donor to recipient cells [34]. Transfer of intact mitochondria via EVs to the recipient cells has been reported, especially during stress and injury [34] and the transferred mitochondria localize within the recipient's mitochondrial network [35], resulting in increased cellular ATP levels [36]. We sought to harness the innate EV

mitochondrial load to increase cellular energetics in ischemic endothelial cells as a potent strategy to protect the BBB, increase its cellular energetics and limit BBB-induced dysfunction post-stroke. We studied the effects of naïve EVs (EXOs and MVs) isolated from a brain endothelial- and macrophage cell lines on the resulting ATP levels in recipient BEC exposed to oxygen-glucose-deprived conditions, mimicking ischemic stroke-like conditions *in vitro*. We demonstrated the feasibility of EVs to deliver ATP5A, an exogenous mitochondrial protein, to increase ATP levels in ischemic endothelial cells. Further, we also investigated if EVs can transfer active and functional (polarized) mitochondria to the recipient BECs.

To the best of our knowledge, we have demonstrated for the *first* time that EVs isolated from a brain endothelial cell line can increase the mitochondrial energetics in the recipient BECs, compared to EVs derived from a macrophage cell line despite their inverse effects in the delivery of DNA to the recipient BECs (macrophage-derived EVs showed a greater transfection compared to the BEC-derived EVs in the recipient endothelial cells). We have also demonstrated, for the *first* time, that BEC-derived EVs transfer functional, polarized mitochondria to endothelial cells in culture and mice acute brain cortical and hippocampal slices. The presented results are of high significance as they demonstrate evidence for the potential of BEC-derived EVs to increase endothelial cell survival under ischemic conditions. Secondly, the capability of EVs to transfer polarized mitochondria to endothelial- and neuronal cells in the brain slices have important implications in the context of ischemic protection.

2. Experimental section

2.1. Materials

Reporter plasmid DNA constructs encoding the firefly luciferase gene (gWIZ-Luc/Luc-pDNA, 6732 bp) and enhanced green fluorescent protein (gWiz-GFP/GFP-pDNA, 5757 bp) were purchased from Aldevron (Fargo, ND). The stock solutions of pDNA were diluted in 10 mM Tris-HCl containing 1 mM EDTA (pH 7.4) to obtain a concentration of 1 mg/mL. The concentration and purity of the diluted solutions were confirmed by measuring A_{260}/A_{280} on a NanoDrop 1000 spectrophotometer (Thermo Scientific, USA). Recombinant Human Adenosine triphosphate synthase subunit alpha (ATP5A)-Glutathione S-transferase (GST) (N-term) full-length recombinant protein was obtained from Novus Biologicals Inc. (Littleton, CO).

Lipofectamine 3000 Reagent kit was purchased from Invitrogen (Carlsbad, CA). Beetle luciferin (potassium salt), and luciferase cell culture lysis 5*x* reagent were purchased from Promega (Madison, WI). Bovine lung aprotinin was purchased from Fisher Bioreagents (New Zealand). Sodium dodecyl sulfate (SDS), Tris-HCl, Tris-base, glycine, methanol, Tween-20, magnesium chloride, ethylenediaminetetraacetic acid disodium salt dihydrate, dithiothreitol, and glacial acetic acid were purchased from Fisher Scientific (Pittsburgh, PA). N,N,N’,N’-tetramethyl ethylenediamine and glycylglycine were purchased from Acros Organics (New Jersey, USA). Protogel 30% acrylamide: 0.8% (w/v) bis-acrylamide stock solution was obtained from National Diagnostics, Atlanta, GA. Adenosine-5’-triphosphate disodium salt hydrate and coenzyme A trilithium salt dihydrate were procured from MP Biomedicals, LLC (Illkirch, France). MitoTracker Deep Red FM and DMSO were purchased from Life Technologies, (Carlsbad, CA). Calcein-AM was purchased from BD Pharmingen BD Biosciences (San Jose, CA). Branched polyethyleneimine (PEI, molecular mass ~ 25 kD) was purchased from Sigma-Aldrich, Saint

Louis, MO. All other chemicals used were of analytical or cell culture grade and were used as received from the manufacturers.

Kits. Pierce Bicinchoninic acid (BCA) and MicroBCA protein assay kits were purchased from Thermo Scientific (Rockford, IL). Quant-iT PicoGreen dsDNA assay kit was procured from Molecular Probes, Inc. (Eugene, OR). CellTiter-Glo-luminescent viability assay reagent was procured from Promega (Madison, WI).

Antibodies. Primary mouse antibody to ATP5A (MW 53 kD) (Catalog #ab14748), rabbit monoclonal antibodies to CD9 (C-4) (MW 22 - 25 kD) (Catalog #ab92726), and rabbit GAPDH polyclonal antibody (MW 36 kD) (Catalog #ab8245) were purchased from Abcam (Cambridge, MA). Alexa Fluor 790-conjugated AffiniPure Donkey Anti Mouse IgG (H+L) was purchased from Jackson ImmunoResearch Lab Inc. (West Grove, PA).

2.2. Cell lines and culture

Immortalized human cerebral microvascular endothelial cell line (hCMEC/D3) was purchased from Cedarlane Laboratories, Burlington, Ontario, Canada (Lot #*1x* 102114.3C-P25). Mouse macrophage cells (ATCC TIB-71, RAW 264.7, Mus musculus) were purchased from ATCC (Manassas, VA).

hCMEC/D3 cells were cultured on well plates or tissue culture flasks pre-coated with 150 μg/mL of collagen (Type 1 Rat collagen fibrillar collagen, 90%, Corning, Discovery Labware Inc., Bedford, MA) diluted in 0.02 N acetic acid. The collagen solution was applied to the tissue culture

flasks or well plates and the culture ware was incubated for 1 h at 37 °C in a humidified incubator. After 1 h, the collagen solution was removed and the surfaces were rinsed with sterile PBS (1*x*, 0.067 M, HyClone, Logan, UT). The hCMEC/D3 cells were cultured in complete media composed of endothelial cell basal medium-2 (Lonza Walkersville Inc., MD), supplemented with 5% heat-inactivated fetal bovine serum (FBS, Hyclone Laboratories, Logan, UT), 10 mM HEPES (pH 7.4) (Fisher Scientific, Pittsburgh, PA), 100 U/mL-100 μg/mL penicillin-streptomycin (Gibco, Carlsbad , CA), 1% chemically defined lipid concentrate (Sigma-Aldrich, Saint Louis, MO), 5 μg/mL ascorbic acid (Sigma-Aldrich), 1.4 μM hydrocortisone (1 mg/mL, Sigma-Aldrich), and 1 ng/mL of recombinant basic fibroblast growth factor (Sigma-Aldrich). RAW 264.7 macrophages were cultured in complete media composed of high-glucose Dulbecco's Modified Eagle's Medium (DMEM (1*x*) containing Glutamax (Gibco, Carlsbad, CA) supplemented with 10% FBS and 1% v/v of penicillin-streptomycin. The culture media was changed after every 2 - 3 days. Conditioned media used for EV isolation was of the same composition except for the lack of FBS to exclude serum-derived EVs.

hCMEC/D3 cells and RAW 264.7 cells were passaged when the cells reached 95-100 % confluency. The hCMEC/D3 cells were detached with Trypsin-EDTA (TrypLE Express 1*x*, Gibco, Denmark) and passaged. The hCMEC/D3 cells were used only between passage numbers 25 and 35. RAW 264.7 cells were passaged by dislodging the adherent cells using a cell scraper. All cells were maintained at 37 ± 0.5 °C in a humidified 5% CO_2 incubator (Isotemp, Thermo Fisher Scientific).

2.3. Isolation of extracellular vesicles (EVs) from hCMEC/D3 endothelial cells and RAW macrophages

For the generation of EVs, hCMEC/D3 cells were seeded in collagen-coated 175 cm^2 tissue culture flasks (Greiner Bio-One GmbH, Frickenhausen, Germany) while RAW 264.7 cells were seeded directly in 175 cm^2 tissue culture flasks containing fresh media and cultured till 90-95% confluency. Upon confluence, the media was carefully removed, and the cell monolayer was gently washed once with 25 mL of pre-warmed sterile PBS and replaced with 25 mL of pre-warmed serum-free media in each flask and cultured in a humidified incubator. After 48 h, the conditioned media was harvested and EVs were isolated by differential centrifugation as described previously [30, 32]. Briefly, the culture supernatant was centrifuged at 300*x*g for 10 min to pellet out the cellular debris. The supernatant was then transferred to fresh tubes and further centrifuged at 2000*x*g for 20 min to pellet out the apoptotic bodies. Following this, the supernatant was carefully collected in polycarbonate tubes (26.3 mL, Beckman Coulter, Indianapolis, IN), and spun at 20,000*x*g for 45 min in a type 50.2Ti rotor (Beckman-Coulter Optima XE-90 ultracentrifuge, Indianapolis, IN) to pellet the microvesicles (MVs). The resulting supernatant from this step was then filtered through a 0.22 μm sterile filter into polycarbonate tubes to remove the larger vesicles and centrifuged at 120,000*x*g for 70 min in a Type 50.2Ti rotor to obtain a pellet of exosomes (EXOs). The pellets containing MVs and EXOs were washed once with sterile PBS and centrifuged again following the procedure described above, i.e., at 20,000*x*g for 45 min and 120,000*x*g for 70 min to isolate the MVs and EXOs, respectively. The entire isolation was conducted at 4 °C. All the EV samples were stored at -80 °C till further use. D3-MVs and –EXOs and RAW-MVs and –EXOs indicate EV subsets obtained from the conditioned media from hCMEC/D3 monolayers and RAW 264.7 cells, respectively. It should be noted our EV isolation

allowed isolating EXOs and MVs as separate fractions, but we collectively refer to the cell-secreted, membranous EXOs and MVs as EVs [37], wherever applicable.

2.4. Measurement of EV protein content

The total EV protein content was measured using a MicroBCA protein assay. EV samples were diluted in 1*x* RIPA lysis buffer containing aprotinin (10 μg/mL) and were kept on ice for 15 min to lyse the EVs. A 150 μL volume of each sample was added to an equal volume of the MicroBCA working reagent in a 96 well-plate and incubated for 2 h at 37 °C per the manufacturer's instructions. Protein concentration was quantified by measuring the absorbance at 562 nm on a microplate reader (Synergy HTX multimode reader, Bio-Tek Instruments Inc.).

2.5. Physicochemical characterization of EVs

2.5.1. Particle diameter and Zeta Potential

The particle diameters and zeta potentials of EVs were measured using Zetasizer Nano (Malvern Panalytical Inc., Westborough, PA) at a EV protein concentration of 0.2 - 0.5 mg/mL at a temperature of 25 °C and a scattering angle of 173°. Particle size distribution was measured in 1*x* PBS while zeta potential was measured in 10 mM HEPES buffer, pH 7.4. All measurements were performed in triplicates. The data are represented as mean ± standard deviation (SD) of triplicate measurements.

2.5.2. Membrane integrity of the isolated EVs

We first ran fluorescent sub-micron size reference beads (Invitrogen, Carlsbad, CA) with mean diameters of 20-, 100-, 200-, and 500-nm on an Attune NxT Acoustic Focusing Cytometer

(Invitrogen, Singapore). The calibration beads allowed the detection of the MVs and EXOs using a 488/10 nm small particle side scatter filter (Invitrogen, Carlsbad, CA) on the BL1 channel and generate a size reference scale. The voltages for forward (FSC-H) and side (SSC-H) scatters were adjusted to 620 V and 240 V respectively and BL1 intensity was adjusted to 380. A total of 5,000 events were acquired for particles within the 100 – 500 nm gate. Threshold on both forward and side scatter channels were set to 0.1 V. EV samples were run at a flow rate of 25 μL/min. Individual EV samples (approximately 50 μL in a volume containing 40 μg – 60 μg of total EV protein) were labelled with 50 μL of 5 μM Calcein-AM (prepared in 10 mM HEPES, 2.5 mM $CaCl_2$, diluted from a reconstituted stock solution of 5 mM Calcein-AM in DMSO) and incubated at 37 °C for 20 min, protected from light and diluted to a final volume of 400 μL in 1*x* PBS immediately before analysis. Control samples included filtered PBS and PBS containing 5 μM calcein AM to rule out any potential noise from the reagent. Triton-X 100 (1 % v/v in PBS) was used to lyse EVs. Freshly isolated EV samples, as well as EV samples stored at different conditions (*a*) frozen at -20 °C for a week, (*b*) samples exposed to three freeze-thaw cycles at -20 °C overnight followed by an ice-thaw for 3 h and (*c*) stored at 4 °C for 3 days, were labelled using calcein to determine EV membrane integrity. The fluorescent signals from the beads and labelled EVs were analyzed using density plots on Attune NxT software.

2.6. Pre-transfection of donor cells with Lipofectamine/DNA complexes and isolation of pDNA-loaded EVs

hCMEC/D3 endothelial cells and RAW 264.7 macrophage cells were first transiently transfected with Lipofectamine-pDNA complexes. The donor hCMEC/D3 or RAW 264.7 cells were seeded at 1.5 x 10^6 cells/well in 24-well plates until 80-100% confluency was achieved.

Lipofectamine 3000-pDNA (Luc-pDNA or GFP-pDNA) complexes or control Lipofectamine alone (no pDNA) were prepared with 1 dose of lipid per manufacturer's protocol (catalog# L300015, Invitrogen, Carlsbad, CA). Cells were transfected such that the pDNA dose was either 0 μg/well (for the generation of naïve EVs), 0.5 μg/well, or 1.0 μg/well (referred to as Luc0.5 or Luc1.0 henceforth) and incubated for 12 h (the total amount of pDNA transfected per 24-well plate were 0, 12, or 24 μg for the indicated groups). The transfected cells were then cultured in serum-free medium for 48 h post-transfection. The conditioned medium was then pooled from each transfection plate and EVs were isolated from each group as described in section 2.3. D3-Luc-MV and D3-Luc-EXO and RAW-Luc-MV and RAW-Luc-EXO indicate the MVs and EXOs isolated from Luc pDNA transfected hCMEC/D3 and RAW 264.7 cells, respectively. Likewise, D3-MV-GFP and D3-GFP-EXO and RAW-GFP-MV and RAW-GFP-EXO indicate the MVs and EXOs isolated from GFP pDNA transfected hCMEC/D3 and RAW 264.7 cells, respectively. For example, RAW-Luc0-MV, RAW-Luc0.5-MV, and RAW-Luc1.0-MV indicate MVs isolated after transfection of parent cells with 0 μg, 0.5 μg, or 1 μg pDNA per well.

2.7. EV protein content in DNA-EVs and quantification of the pDNA content in DNA-EVs

The protein content of the EVs in the DNA-EVs was determined using MicroBCA assay as described in 2.4. The amount of double-stranded DNA in the DNA-EVs was measured using the Quant-iT PicoGreen dsDNA assay kit following the manufacturer's protocol. DNA-EVs were lysed in 1*x* RIPA buffer containing aprotinin (10 μg/mL) on ice for 30 min followed by dilution in 1*x* TE buffer to make up the volume up to 100 μL. The volumes of EV suspension were adjusted so that it stayed within the standard curve range (0 μg – 1000 μg of calf thymus DNA/200 μL of assay volume). A 100 μL volume of the diluted Picogreen reagent was added to 100 μL of the EV

samples in a black 96-well plate. The contents were mixed in a shaker incubator for 5 min at room temperature in the dark and fluorescence was measured using a microplate reader at excitation and emission wavelengths of 485 and 528 nm, respectively (Synergy HTX multimode reader, Bio-Tek Instruments Inc., USA). The percent of DNA loading in the isolated EVs was calculated using **Equation 1**.

$$DNA\ Loading\ (\%) = \frac{(Amount\ of\ DNA\ \ in\ DNA{-}EVs - amount\ of\ DNA\ \ in\ naive\ EVs\ )}{Total\ amount\ of\ DNA\ \ transfected\ into\ the\ donor\ cells} \times 100\% \quad \textit{Equation 1}$$

2.8. DNA-EV transfection in the recipient brain endothelial cells (BECs)

The transfection activity of Luc DNA-EVs was measured using a luciferase assay. hCMEC/D3 cells were first seeded into collagen-coated 48-well plates at a density of 55,000 cells/well. When the cells reached approximately 80% confluency, the media was freshly replaced with 150 µL of complete medium. D3-Luc-MV; D3-Luc-EXO; RAW-Luc-MV; and RAW-Luc-EXO, each containing 10 ng of DNA were added to each well and incubated for 24 h, 48 h, and 72 h. Untreated hCMEC/D3 cells and cells transfected with Lipofectamine complexes containing 10 ng of Luc-pDNA were used as controls. Post-24-, 48-, and 72 h transfection with Luc-EVs, the transfection medium was discarded. The cells were washed with PBS followed by the addition of 100 µL of 1*x* Luciferase cell culture lysis reagent in each well and mixed thoroughly on a shaker for 20 min at room temperature followed by four freeze-thaw cycles (-80 °C for 60 min and 4 °C for 60 min) to completely lyse the cells. The luciferase assay was conducted as previously described by us [32, 38]. The total cellular protein content was quantified using a BCA protein assay using the manufacturer's protocols. Luciferase expression was expressed as relative light units normalized

to total cellular protein (RLU/mg protein). The RLU/mg of protein content for each group was further normalized to untreated cells.

2.9. Proteomics analysis of EVs

EVs (25 μg) were electrophoretically separated on 4%-10% Tris-HCl gel. The proteins were visualized using a Bio-Safe Coomassie Blue G-250 stain. The gel lanes were cut into 0.5 mm x 5 mm bands.

In-gel trypsin digestion

In-gel trypsin digestion was carried out as previously described [39]. Briefly, gel bands were diced into small pieces (<1 mm^3) and washed with a solution of 50% acetonitrile/ 25 mM ammonium bicarbonate until no more visible stain was present. The gel pieces were then dehydrated with 100% acetonitrile (ACN), reduced with 10 mM dithiothreitol (DTT) at 56 °C for 1 h, followed by alkylation with 55 mM Iodoacetamide (IAA) at room temperature for 45 min in the dark. Excess DTT and IAA were removed by washing the gel pieces with 25 mM ammonium bicarbonate and then twice with 100% ACN. A solution containing 20 ng/μL sequencing grade modified trypsin (Promega Corporation, Madison, WI; catalog#V511A) and 25 mM ammonium bicarbonate was added to cover the gel pieces and digestion was carried out overnight at 37 °C. The resultant tryptic peptides were extracted from the gel with 70% ACN/5% formic acid (FA), vacuum dried, and reconstituted in 18 μL 0.1% FA for nanoflow liquid-chromatography tandem mass spectrometry (nLC-MS/MS) analysis.

Tandem Mass Spectrometry

Tryptic peptides were analyzed by nLC-MS/MS using a NanoAcquity UPLC (Waters' Corporation, Milford, MA) interfaced to a Velos Pro linear ion trap mass spectrometer (Thermo Fisher Scientific, Waltham, MA). For each analysis, a 1 µL volume of protein digest was injected onto a C18 column (PicoChip column packed with Reprosil C18 3µm 120 Å chromatography media in a 10.5 cm long, 75 µm ID column with a 15 µm tip, New Objective, Inc., Woburn, MA) and then eluted off to the mass spectrometer using a 37-minute linear gradient of 3-35% ACN/0.1% FA at a flow rate of 300 nL/min.

The Velos Pro was operated in positive ionization mode with a spray voltage of 1.95 kV and capillary temperature of 275 °C. The acquisition consisted of cycles of one full-scan MS1 (AGC of $3x10^4$, 75 ms maximum ion accumulation time, and m/z range of 375-1800) followed by eight MS/MS spectra recorded sequentially for the most abundant ions in the ion trap (minimum signal required 1000 counts, $1x10^4$ AGC target, 100 ms maximum injection time, isolation width 2 m/z, normalized collision energy 35, and activation time 10 ms). Dynamic exclusion (30 s) was enabled to minimize the redundant selection of peptides previously selected for MS/MS.

Data Analysis

Collected MS/MS spectra were searched using the MASCOT search engine v2.4.0 (Matrix Science Ltd., London, England) [40] against a Swissprot Homo sapiens database (downloaded on 04/25/2019; 42439 entries) for the human samples and a Uniprot Mus Musculus database (downloaded 01/19/2019; 94376 entries) for mouse samples. The mass tolerance was set to 1.4 Da for the precursor ions and 0.8 Da for the fragment ions. Peptide identifications were filtered using the PeptideProphet and ProteinProphet algorithms with a protein threshold cut-off of 99%,

minimum of 2 peptides, and peptide threshold cut-off of 90% implemented in Scaffold v4.11.0 (Proteome software, Portland, OR).

2.10. Mitochondrial transfer from EVs to the recipient brain endothelial cells

2.10.1. Isolation of EVs from source/donor cells pre-labelled with MitoTracker Deep Red FM

Confluent 175 cm^2 tissue culture flasks containing hCMEC/D3 cells or RAW 264.7 cells were washed with pre-warmed PBS followed by incubation with 250 nM of MitoTracker Deep Red FM (MitoT) (diluted in the respective growth medium) for 30 min at 37 °C in the dark. The dye-containing medium was then replaced with their respective complete medium and further incubated at 37 °C for 1 h, followed by washing with PBS and incubation with serum-free medium for 16 h. The conditioned media was then subjected to ultracentrifugation as described in section 2.3 to isolate EVs. The isolated pellets were resuspended in 1 mL of sterile PBS. D3-MitoT-MV and D3-MitoT-EXO and RAW-MitoT-MV and RAW-MitoT-EXO indicate the MVs and EXOs isolated from MitoT-labelled hCMEC/D3 and RAW 264.7 cells, respectively. The protein content in MitoT-EVs was determined using a MicroBCA assay.

2.10.2. Treatment of the recipient endothelial cells using MitoT-EVs

Confluent 48-well plates of hCMEC/D3 cells were prepared as described earlier. The cells were then incubated with D3-MitoT-MV, D3-MitoT-EXO, RAW-MitoT-MV, and RAW-MitoT-EXO at different protein amounts viz., 3, 12, 24, 50, 100, and 200 μg per well. The plates were incubated for 24, 48, and 72 h at 37 °C in the dark. After incubation, the media was replaced with a phenol red-free DMEM medium. The cells were observed under an Olympus IX 73 epifluorescent inverted microscope (Olympus, Pittsburgh, PA) to detect MitoT signals using the

Cyanine-5 (C) channel (Cy5, excitation 635/18 nm and emission 692/40 nm) and under phase contrast settings at 20x magnification. The images were processed using cellSens dimension software (Olympus, USA) and Image J software (NIH). Cell monolayers stained with 250 nM MitoT for 30 minutes in dark were used as a positive control to detect MitoT signals and unstained cells were used as an additional control. Image contrast was adjusted using ImageJ (NIH).

2.10.3. Uptake of MitoT-EVs into mice acute brain slices

Acute Brain Slice Preparation

The Institutional Animal Care and Use Committee (IACUC) at the University of Colorado approved all experimental protocols in accordance with the National Institutes of Health and guidelines for the care and use of animals in research. Adult (20–25 g) male C57Bl/6 (8–12 weeks) mice purchased from Charles River Laboratory (Fredrickson, NC) were used for this study. All mice were housed in standard 12-h light dark cycle with free access to food and water. All experiments in the study adhered to the ARRIVE guidelines for animal experiments. Following middle cerebral artery occlusion sham surgery [41-43], mice were anesthetized with isoflurane (3%) and transcardially perfused with artificial cerebral spinal fluid (ACSF: 126 mmol/L NaCl, 2.5 mmol/L KCl, 25 mmol/L $NaHCO_3$, 1.3 mmol/L NaH_2PO_4, 2.5 mmol/L $CaCl_2$, 1.2 mmol/L $MgCl_2$, and 12 mmol/L glucose, pH 7.4) oxygenated with 95% O_2/5% CO_2 and at ice-cold conditions (2–5°C) for 2 min before decapitation. Brains were removed and horizontal cortical or hippocampal sections (300 μM thick) were cut in ice-cold ACSF using a VT1200S Vibratome (Leica, Buffalo Grove, IL, USA) and were recovered in ACSF for 30 minutes at 37 °C before treatment with MitoT-EVs.

Incubation with MitoT-EVs

Acute brain slices were incubated in 50 µg/mL of D3-MitoT-EXO and D3-MitoT-MV diluted in normal ACSF for 2 h at 37°C, and counterstained using Hoechst 33258. Non-incubated slices were used as a negative control. The slices were fixed in 4 % of paraformaldehyde overnight at 4°C and were washed in PBS prior to mounting. The slices were imaged using a confocal microscope (Olympus FV1000 laser scanning confocal microscope) equipped with an Olympus Fluoview imaging software (Center Valley, PA, USA) under the cyanine-5 channel (Cy5, excitation 651 nm and emission 670 nm) for visualizing MitoT signals.

2.11. Effects of EV exposure on the cell viability of the recipient BECs

2.11.1. Effect on normoxic BEC cultures

We determined the effects of EV exposure using the CellTiter-Glo luminescent cell viability assay following the manufacturer's protocol. Briefly, hCMEC/D3 cells (16,000/well) were seeded in 96-well plates for 24 h in 200 µL of D3 complete media at 37 °C and 5% CO_2 in a humidified incubator. After confluency, the complete media was replaced with fresh media containing EVs at different protein doses (in a total volume 100 µL/well) and incubated for 72 h. The resulting ATP/cell viability levels in each group was measured as discussed in the following section 2.11.2.

2.11.2. Effect on hypoxic BEC cultures

BECs were exposed to oxygen-glucose deprivation (OGD) as follows: confluent hCMEC/D3 monolayers were washed with pre-warmed PBS, and replaced by glucose-free media as described in [44] and placed in a hypoxia chamber (Billups-Rothenberg, CA, USA) saturated with a 5-7 min flush of 90% N_2, 5% H_2, 5% CO_2 (25 l/min). The sealed hypoxic chamber was kept at 37 °C in a

humidified incubator. Different periods of OGD exposure were evaluated to induce endothelial cell death. After exposure of the 96-well plates to the optimized OGD time of 4 h, the media was replaced with 100 μL of OGD medium containing EVs suspended in PBS containing varying amounts of total EV protein and incubated in normoxic conditions (in a humidified 5% CO_2 incubator) for the indicated times. Healthy cells (non-OGD) cultured under normoxic conditions (~100% viability) and OGD-exposed cells subsequently cultured in normoxic conditions (~0% viability) were used as controls. Post-treatment with EVs, cells were washed with pre-warmed PBS followed by the addition of 60 μL of complete growth medium and 60 μL of CellTiter-Glo 2.0 assay reagent to each well. The wells were incubated in a shaker at room temperature for 15 min in the dark. After 15 min, 60 μL of the solution from each well were aliquoted into an opaque, white 96-well plate luminescence plate (Fisherbrand). Relative luminescent signals were measured using Synergy HTX multimode reader (Bio-Tek Instruments Inc., USA) at 1 sec integration time. The relative cell viability (%) was calculated after normalizing the relative luminescence units (RLU) of treated cells to those untreated cells as shown in **equation 2**.

$$Relative\ cell\ viability\ (\%) = \frac{RLU\ from\ group\ treated\ with\ EVs\ or\ PEI}{RLU\ from\ untreated\ cells\ or\ untreated\ OGD\ cells} * 100 \qquad Equation\ 2$$

2.12. Formation of EV-ATP5A protein complexes

Complexes of recombinant ATP5A1 protein were formed with the EVs by mixing naïve EVs (EXOs/MV 1:1 mixture) and ATP5A at an EV:ATP5A protein weight/weight (w/w) ratio of 5:1. Precalculated volumes of ATP5A solution were added slowly along the walls of the microtube containing EVs diluted in 1*x* PBS. The complexes were prepared by mixing these solutions and vortexed at a setting of ‘5’ on a vortex mixer (Fisher Analog Vortex, 120V, Fisher Scientific, USA)

for 30 secs. After mixing, the tubes containing the complexes were spun down for five seconds and allowed to stand at room temperature for 30 min prior to use in experiments.

2.12.1. Native gel electrophoresis

The formation of the EV-ATP5A complexes was confirmed by native polyacrylamide gel electrophoresis. Free ATP5A protein, naïve EV samples, or EV/ATP5A complexes were mixed with an equal volume of native sample buffer (BioRad) and resolved on 4-10% gel in 25 mM Tris, 192 mM Glycine, pH 8.3 at 100 V for 2 h. The gels were then stained with Bio-safe Coomassie Stain solution overnight before scanning using an Odyssey imager (LI-COR Inc., Lincoln, NE) at the 800 nm near-infrared channel.

2.12.2. Effect of the exposure of EV/ATP5A complexes on the ATP levels in the recipient endothelial cells

ATP5A doses of 100, 200, and 300 ng per 0.32 cm^2 of 96-well plate were used in these studies. The EV-ATP5A complexes were diluted in OGD media before addition to cells 4 h post-OGD exposure. The cells were incubated with the indicated samples for 4 h, washed with pre-warmed PBS, and resulting ATP levels were determined by CellTiter Glo assay (as described in section 2.11.2). The effects of the treatment were expressed as the resulting ATP levels compared to the untreated OGD cells subjected to reoxygenated/normoxic conditions for 4 h. Relative luminescent signals were measured using Synergy HTX multimode reader (Bio-Tek Instruments Inc., USA) at 1 sec integration time. The relative cell viability (%) was calculated after normalizing the relative luminescence units (RLU) of treated cells to those untreated cells as shown in **equation 3**.

$$ATP\ levels\ (\%) = \frac{RLU\ from\ treated\ cells}{RLU\ from\ untreated\ OGD\ cells} * 100 \qquad Equation\ 3$$

2.13. Statistical analysis

The number of independent experiments for each study is indicated in each figure or table legend. Each experiment was repeated at least thrice to confirm data reproducibility. The results are expressed as mean ± standard deviation (SD). Comparative analyses were performed using either one-way or two-way ANOVA using GraphPad Prism v8 (GraphPad Software, San Diego, CA). Wherever applicable, one-way ANOVA was done using Bonferroni's multiple comparisons test. Alpha was set at 0.05.

3. Results and Discussion

The innate cargo of EVs is comprised of membrane and vesicular proteins, lipids, and a variety of nucleic acids such as mRNA, non-coding RNAs, microRNA, ribosomal RNA, etc. [26, 45, 46]. As a result of their rich RNA load, EVs naturally sparked an interest as carriers for the delivery of exogenous nucleic acids. The presence of DNA fragments ranging in sizes from 1 to 20 kb have also been reported in EVs [47-49]. A small number of published reports demonstrated the loading of plasmid DNA in EVs [30-32]. Though electroporation permitted the loading of DNA into EVs, the levels of loading were severely limited by their large molecular sizes [31]. Lamichhane *et al.* demonstrated the effect of DNA size, both linear and circular DNA, on the loading efficiency of the EVs. Linear dsDNA of 250 bp was maximally loaded into EVs at a dose of 5 μg via electroporation. However, the same electroporation approach could not load plasmid DNA and linear DNA greater than 1000 bp [31]. The key overarching challenge identified in these papers was the fact that the levels of DNA loading were very low at about < 0.2 %.

The objectives of the current study are two-fold: as described in the introduction section, we first sought out to re-confirm our previous results on the DNA loading and transfection of EVs from two different parent cell sources: brain endothelial cells (BECs) vs. macrophages to eliminate any operator-induced systematic biases. In this study, we also conducted proteomic analysis to identify a possible reason for the greater transfection of the heterotypic, macrophage-derived EVs instead of the homotypic, BEC-derived EVs into the recipient BECs. The second goal of this study was to determine the potential effects of the EV mitochondrial load on the cellular energetics in the recipient ischemic endothelial cells. In our previous study, we surprisingly observed a higher Luc-DNA loading in the EVs derived from RAW 264.7 macrophages (when the cells were pre-transfected with a lower 0.5 µg DNA/well compared to a higher 1.0 µg DNA/well dose) compared to BEC-derived EVs [32]. In addition, we also observed a higher DNA loading in the smaller exosomes (EXOs) compared to the larger microvesicles (MVs)—this finding was in direct contrast to the findings previously by Kanada *et al.* who reported that while EXOs failed to show expression of the reporter protein encoded by the exogenous pDNA, the larger MVs showed transfer and subsequent expression pDNA-encoded reporter protein in the recipient HEK293FT cells [30]. To rule out any unintentional, operator-induced biases in the experimental regime, an independent operator repeated the donor cell transfection and isolated DNA-loaded EVs from the brain endothelial and macrophage cell lines. We compared the physicochemical characteristics of the DNA-loaded EVs, transfection activities in the recipient endothelial cells and used proteomic analyses to identify the possible reason for why the heterotypic, macrophage-derived EVs showed a greater transfection compared to the homotypic, BEC-derived EVs in the recipient BECs.

The brain endothelial cells have higher metabolic activity compared to the other non-brain endothelial cells [50]. Under ischemic/hypoxic conditions, the endothelial cells are susceptible to undergo apoptosis resulting in increased mitochondrial dependence for metabolism and survival [51]. During the biogenesis of EVs, mitochondria, mitochondrial proteins, or mitochondrial DNA are incorporated into these vesicles and can be transferred between cells [34]. Depolarized mitochondria can be transferred to cells under oxidative stress via MVs resulting in enhanced bioenergetics and cell survival of the recipient cells [34]. Mouse bone marrow-derived stromal cells derived MVs transferred mitochondria and increased the alveolar ATP levels in lipopolysaccharide-exposed mice lungs [36]. Airway myeloid-derived regulatory cells-derived EXOs have also been reported to transfer mitochondria to T cells and localize with the T cell's mitochondrial network [35].

The objective of our work is to determine if the EV mitochondrial load can be transferred to ischemic endothelial cells in an *in vitro* oxygen-glucose deprivation model of stroke and to neurons in mice acute brain slices. The lack of ATP serves as the initial trigger in the ionic, biochemical, and cellular events that cause death and damage during stroke [8]. We, therefore, hypothesized that the transfer of innate EV mitochondria may switch the endothelial cell fate from death to survival. The underlying rationale for our hypothesis is that protecting the BECs lining the BBB will subsequently allow it to maintain its barrier properties and limit BBB dysfunction-induced neurological damage in diseases like stroke.

3.1. Isolation and characterization of hCMEC/D3 endothelial cell- and RAW 264.7 macrophage-derived EVs

As previously reported by us [32], a cell model of the human BBB, hCMEC/D3 endothelial cells, and RAW 264.7 macrophages were used to compare if the donor/source cell line has any effects on the extent of DNA loading for subsequent transfection into the recipient endothelial cells. Neither the hCMEC/D3 endothelial (abbreviated as D3) nor the RAW264.7 macrophages (abbreviated as RAW) showed substantial changes in morphology when cultured under serum-free conditions (**Fig. S1**). Naïve EVs isolated from hCMEC/D3 endothelial and RAW 264.7 macrophage cells showed average particle diameters ranging between 100 to 250 nm as shown in **Fig. 1b-e**. We noted a significant difference among the average particle diameters for EXOs and MVs isolated from both cell sources. D3-EXO, D3-MV, and RAW-EXO showed heterogeneous size distributions as expected for cell-derived vesicles. A smaller fraction of EXO sized <100 nm was seen in D3-EXO while D3-MV and RAW-EXO showed particle populations >150 nm. MVs are known to be heterogeneous in size with effective particle diameters ranging from 200 - 1500 nm [52, 53]. The overall sizes of EXOs and MVs isolated from both cell lines were in agreement with previous studies [30]. These size ranges suggest the increased likelihood of EVs entering recipient cells via endocytosis [54]. The zeta potentials of EV samples ranged between -4 and -12 mV (**Fig. 1a**). The negative zeta potential is attributed to their anionic

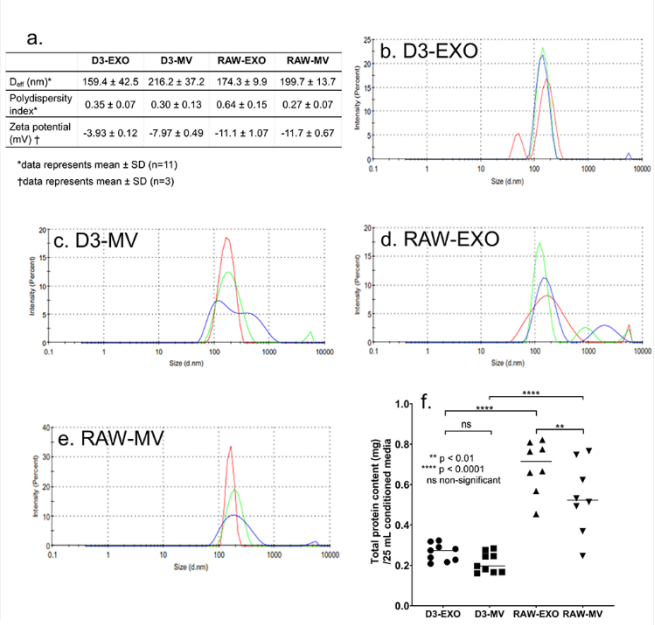

	D3-EXO	D3-MV	RAW-EXO	RAW-MV
D_{eff} (nm)*	159.4 ± 42.5	216.2 ± 37.2	174.3 ± 9.9	199.7 ± 13.7
Polydispersity index*	0.35 ± 0.07	0.30 ± 0.13	0.64 ± 0.15	0.27 ± 0.07
Zeta potential (mV) †	-3.93 ± 0.12	-7.97 ± 0.49	-11.1 ± 1.07	-11.7 ± 0.67

*data represents mean ± SD (n=11)
†data represents mean ± SD (n=3)

Figure 1. Characterization of EVs derived from hCMEC/D3 (D3-EXO and D3-MV) and RAW 264.7 cells (RAW-EXO and RAW-MV).

membrane lipids like phosphatidylserine and glycosylated proteins that are incorporated into the EXOs and MVs during their biogenesis [55, 56].

The protein yields of EXOs and MVs derived from hCMEC/D3 and RAW 264.7 cell lines are shown in **Fig 1f**. The protein content of EVs derived from RAW 264.7 macrophages was significantly higher than those derived from hCMEC/D3 endothelial cells (*p<0.001*). The number of EVs produced by cells varies and depends upon the parent/donor cell origin. For instance, tumor cells produce more EVs compared to normal cells [57]. RAW 264.7 are leukemic monocyte/macrophage-like cells with a doubling time of approximately 15 h while hCMEC/D3 is a model of brain endothelial cells with a doubling time of approximately 24 h [58]. In addition to that, RAW macrophages have a smaller cell volume compared to the spindle-shaped BECs (**Fig. S1**). Therefore, it is reasonable to expect that confluent macrophages produce more EVs compared to a confluent monolayer of D3 endothelial cells. The protein content of RAW-EXOs was ca. 1.3-fold greater than that of RAW-MVs. It is known that the shedding of MVs is a highly regulated and energy-dependent process occurring more frequently in tumor cells. Moreover, the release rate of MVs is influenced by the presence of serum growth factors in the culture medium which in turn increases the intracellular calcium that is responsible for vesicle shedding [52, 59, 60]. It should be noted that we isolate EVs from a “conditioned” medium that lacks serum to avoid collecting serum-derived EXOs. This likely explains the slightly lower yields of MVs than the EXOs. On the other hand, EXOs can be secreted spontaneously but its concentration is regulated by EXOs already present in the extracellular environment [57, 59].

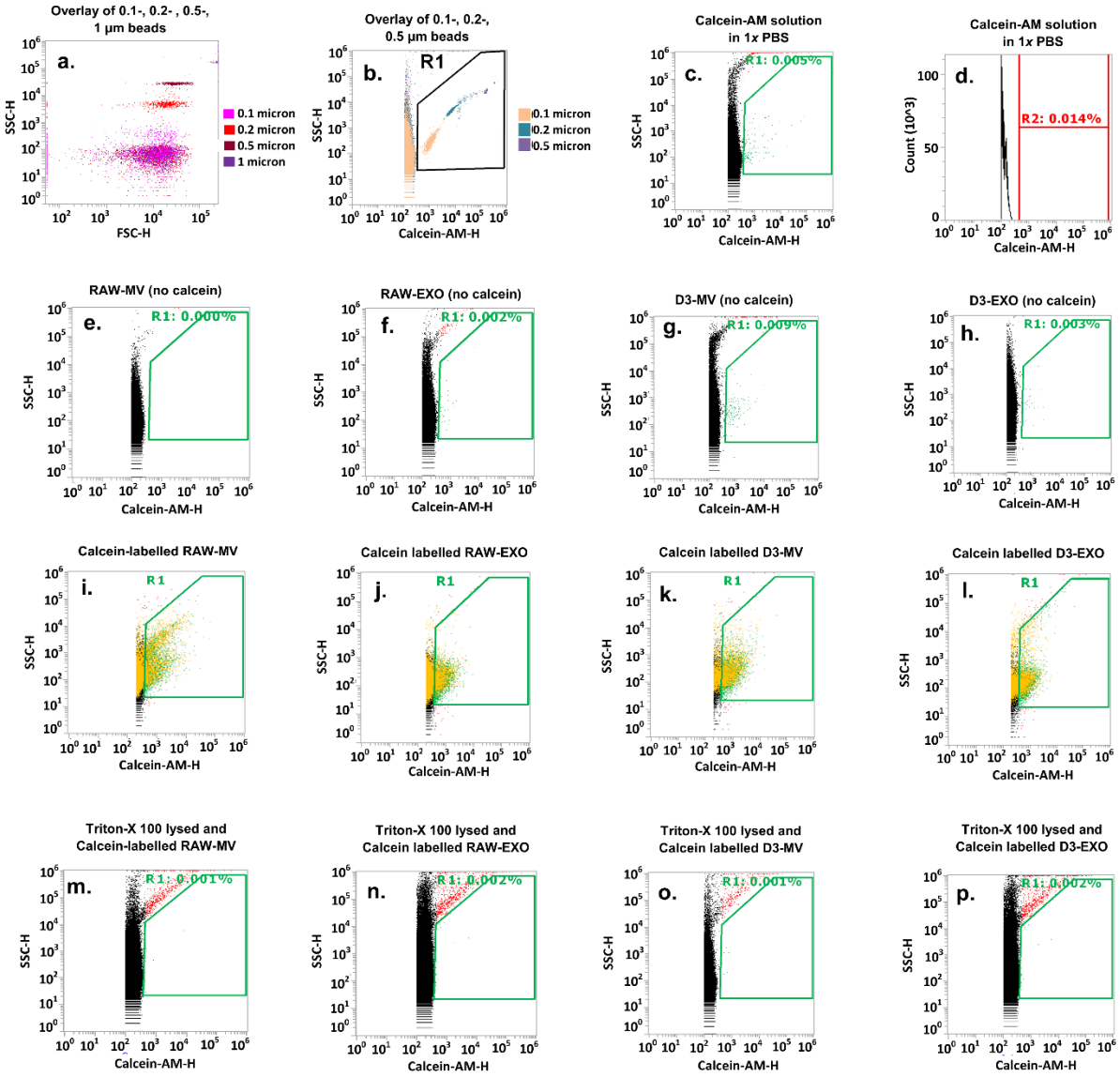

Figure S2: Flow cytometry analysis of EVs.

The integrity of EV membranes and were determined using flow cytometry using previously reported methods [61, 62]. Calcein AM is a non-fluorescent, membrane-permeable dye that undergoes hydrolysis by intravesicular esterases present only in an intact vesicle [63]. Derivatives of calcein especially its acetomethoxy derivative (Calcein-AM) have been extensively studied for live cell tracking and detection. This has also been applied to distinguish functional and metabolically-active EVs from the disrupted EV or protein debris [64]. Fluorescent sub-micron

size reference beads with mean diameters of 20-, 100-, 200- , and 500-nm were used to generate a size reference scale. Gating was applied to exclude the background laser noise in the scatter plots [64]. The detection gate was set between 100 and 500 nm to allow the detection of the beads alone (**Fig. S2a,b**). Gated events for EVs (R1) corresponding to the free calcein-AM solution in 1*x* PBS (**Fig. S2c,d**) and non-stained EVs (**Fig. S2e-h**) were used as controls. Additionally, an EV sample lysed using 1% (v/v) of Triton X-100 was used as a negative control. As expected, no positive events for EVs were observed following the treatment of EVs with Triton X-100 (**Fig. S2m-p**).

Viable RAW-MV (**Fig. S2i**), RAW-EXO (**Fig. S2j**), D3-MV (**Fig. S2k**), D3-EXO (**Fig. S2l**) with calcein positive counts were noted to be present corresponding to particle diameters ranging from 100 to 200 nm. This correlates with our DLS data wherein the mean effective particle size diameters of D3-EXO and D3-MVs ranged from 160 - 250 nm. Lucchetti *et al.* also reported 100 nm-sized EXOs with a refractive index less than 1.4 based on the side scatter signal intensity compared to the 100 nm polystyrene beads (refractive index of ~1.6) [64].

To investigate the effect of storage conditions on the integrity of EV membranes, EV samples were stored at -20 °C and 4 °C for different periods until analysis and compared to the control, freshly-isolated EV samples. From the SSC/FSC scatter profile it appeared that their sizes were comparable to the control, but the number of EV events was significantly altered. After storage for 3 days at 4°C, the number of EV events for D3-EXO was markedly lower compared to the control (**Table 1**). Freezing the EVs at -20 °C retained the number of EV events better than those samples that were subjected to three freeze-thaw cycles (frozen thrice at -20 °C followed by thawing for 3

h at 4°C). The stability of EVs as a function of their membrane integrity was calculated using the **equation 4**.

Stability of EVs at the test storage condition (%) was calculated using the following equation:

$$\frac{\textit{Number of EV events in the sample at the indicated storage condition} - \textit{Number of EV events in a freshly isolated EV sample}}{\textit{Number of EV events in a freshly isolated EV sample}} \text{x100} \quad \text{Equation 4}$$

Table 1. Stability of EVs upon storage at different conditions

	Stability of EVs upon storage at the indicated conditions		
Sample	**4 °C for 3 days**	**-20 °C for 1 week**	**Freeze-thawed thrice at - 20 °C followed by a thaw of 3 h on 4°C**
	(%)	**(%)**	**(%)**
D3-EXO	61.9 ± 9.3	106.7 ± 16.1	82.7 ± 29.6
D3-MV	77.7 ± 16.7	105.7 ± 24.7	89.5 ± 26.0
RAW-EXO	75.1 ± 13.6	95.7 ± 23.7	98.1 ± 6.3
RAW-MV	58.6 ± 12.7	107.7 ± 21.4	89.9 ± 16.3

It can be noted that in some samples, the number of EVs events were higher than the control sample. A similar observation was seen earlier in [62], wherein the number of MV events were higher upon storage at -80 °C with a simultaneous decrease in the size of MVs, the mechanism for which is not known. Similarly, a variation and a trend towards an increase in EV count were observed upon storage at – 20 °C and – 80 °C by Jeyaram and colleagues [65]. This could be due to a shift in the EV size upon storage at -20 °C [65] probably due to structural change of the EVs [66]. Lőrincz *et al.* suggested that the swelling of vesicles upon storage may have caused more of the smaller-sized vesicle fraction to be detected in the preset gated region of the scatter plots [66]. We therefore used freshly isolated EVs in all our studies.

3.2. DNA-loaded EVs derived from hCMEC/D3 endothelial cells and RAW 264.7 macrophages

As previously reported by us [32], we used a passive transfection-based approach to engineer the EVs using Luc-pDNA as a model plasmid. We used Lipofectamine:pDNA ratios of 1:1 to transfect the parent cells to avoid any side effects of excess/free lipofectamine. The non-specific toxicity of cationic lipids [67], their potential to alter the cell gene expression, and their potential effects to alter the innate EV cargo [68] cannot be ignored. Therefore, we used the minimally-required amount of lipofectamine to transfect pDNA into the parent cells while varying the amount of Luc DNA – 0.5 or 1.0 µg (Luc0.5 or Luc1.0), transfected into the parent cells. We used a Quant-iT Picogreen assay to determine the dsDNA loading in the EVs isolated from hCMEC/D3 endothelial cells and RAW 264.7 macrophages.

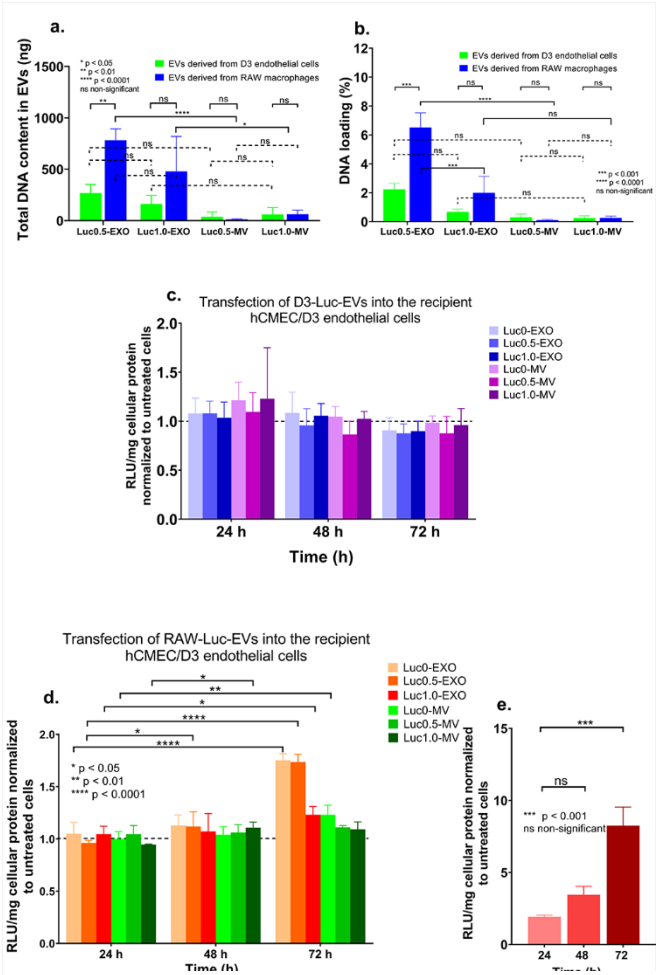

Figure 2. Measurement of DNA content in Luc pDNA-loaded EVs derived from hCMEC/D3 endothelial cells and RAW 264.7 macrophages and their transfection activity in the recipient hCMEC/D3 endothelial cells.

Consistent with our previous findings, our data showed that the RAW-Luc-EXO loaded more DNA than the D3-Luc-EXO ($p < 0.005$ for Luc0.5) compared to the RAW-Luc-MV and D3-Luc-MV. Moreover, RAW-Luc-MV revealed no significant difference in their DNA loading at both the DNA doses of 0.5 and 1.0 µg/well compared to D3-

Luc-MV at their respective doses (**Fig. 2a**). However, Luc-pDNA loading in RAW-Luc0.5-MV was significantly lower ($p < 0.001$) than RAW- Luc0.5-EXO. The percent DNA loading (**Fig. 2b**) was calculated using **equation 1**. Both D3-Luc0.5-EXO and RAW-Luc0.5-EXO showed almost a three-fold increase in the percent DNA loading compared to D3-Luc1.0-EXO and RAW-Luc1.0-EXO. No significant differences were noted in the extent of DNA loading in MVs derived from hCMEC/D3 endothelial and RAW 264.7 macrophage cells. The maximum level of DNA loading was observed in RAW-Luc0.5-EXO (approximately 6.5%) followed by RAW-Luc1.0-EXO and D3-Luc0.5-EXO [54, 69].

The reproducible observations of higher pDNA-Luc loading in RAW-derived EVs may likely be due to the fact that brain endothelial cells possess high intrinsic resistance to transfection compared to the other cell lines even while using the potent non-viral transfection agents [70, 71] and as a result, BEC-derived EVs also concomitantly load lower amounts of the transfected DNA. We also posit that as EXOs are endosomal-derived vesicles compared to the membrane-derived MVs, there is a greater likelihood that the lipofectamine/DNA complexes (that are known to be internalized via endocytosis) or part of the released DNA were entrapped in these EXOs compared to MVs. In other words, there is a natural overlap between the subcellular trafficking of the lipofectamine/DNA complexes and the biogenesis of exosomes. This natural overlap may allow a greater loading of the exogenous DNA into the smaller EXOs compared to the larger MVs that bud off from plasma membranes. Therefore, from two independent studies conducted by independent operators in our lab ([32] and the current study), we conclude that the smaller EXOs loaded a greater amount of exogenous pDNA compared to the larger MVs. Noteworthy, EV production and release into the culture medium is a dynamic process that depends upon the

production rate and the recycling and reuptake rates of EVs back into the cells [57]. This may have resulted in lower pDNA loading in the slow-dividing hCMEC/D3-derived EVs than those derived from rapidly-dividing RAW 264.7 macrophage cells.

Consistent with our previous observations, the loading efficiency of pDNA in the EVs was independent of the pDNA dose transfected into the donor/source cells (0.5 vs. 1 μg/well). An increase in the transfected pDNA dose (Luc1.0-EXO or Luc1.0-MV) did not result in a measurable increase in DNA transfer or the resulting luciferase protein expression compared to Luc0.5-EXO or Luc0.5-MV groups derived from both the cell lines. It has been reported that the loading of DNA into EVs is dependent upon the size of the DNA construct used [31]. Electroporation has shown maximal DNA loading levels of ~2% for 750 bp DNA. Lamichhane *et al*. reported that linear dsDNA molecules of 250 bp were loaded into the EVs efficiently via electroporation at a maximum amount of 5 μg linear dsDNA [31]. Their data showed that approximately 50 ng of DNA was loaded in 3 x 10^8 EVs when an initial amount of 2.5 μg of linear dsDNA was used [31]. Plasmid DNA and linear DNA greater than 1000 bp were not loaded using the electroporation approach. The suggested plasmid DNA cut-off is ~ 4.5 to ~10 kb albeit the loading efficiencies were < 0.2% [31]. The size of the plasmids used in the study was 6.7 kb and 5.8 kb for Luc-pDNA and GFP-pDNA, respectively. The DNA loading in D3-GFP0.5-EXO and D3-GFP1.0-EXO was 0.58 % and 0.36 % respectively, while that in D3-GFP0.5-MV and D3-GFP1.0-MV were 0.11 % and 0.10 % respectively. As observed in the EVs loaded with Luc-pDNA, the EXOs showed a greater DNA loading capacity compared to MVs. Likewise, the DNA loading in RAW-GFP0.5-EXO and RAW-GFP1.0-EXO was 0.29% and 0.48% respectively, while that in RAW-GFP0.5-MV and RAW-GFP1.0-MV were 0.36% and 0.36% respectively. MVs derived from both the cell

lines showed an insignificant gradual increase in exogenous DNA (from 0/naïve EVs to 1 µg/well) and are likely due to the variations in DNA loading that correlates with their biogenesis pathways as discussed in the previous paragraph. Interestingly, our results contradicted previously published reports [30, 31], that suggested that MVs showed a greater potential for transfection compared to EXOs due to increased DNA loading; although Lamichhane *et al*. did not observe measurable transfection of the DNA-EVs.

The differences in DNA loading between EXOs and MVs may also be explained because EXOs have less endogenous or innate cargo. A proteomics study comparing the protein content of EXOs and MVs reported that MVs are enriched with proteins related to the cytoskeletal network and cortical activity compared to the EXOs [72]. Moreover, if MVs are released through a regulated, generally low, steady-state process as compared to EXOs that are released constitutively [73], the biogenesis of MVs loaded with DNA will also be comparatively lower. No significant changes in the total EV protein content were observed with DNA-loaded EVs and EVs isolated from cells treated with lipofectamine alone (no DNA). This indicated that the biogenesis and release of EVs were not unaffected due to the transfection process using cationic lipids (lipofectamine) at the different pDNA amounts. We further compared the particle diameters of naïve vs. DNA-loaded EVs (**Table 2**) to determine if those differences could explain the lower transfection levels of DNA-MVs compared to DNA-EXOs despite both carriers containing an equivalent amount of pDNA, 10 ng. We prepared EVs loaded with both luciferase (luc) and eGFP (GFP) pDNA to determine if the type of the pDNA construct affected their particle characteristics. It is well-documented that the physicochemical characteristics of nanoparticle carriers strongly affect their biological activity *in vitro* [38, 74, 75]. We noted that the effective particle diameters

of DNA-EVs derived from hCMEC/D3 cells were somewhat unchanged with a slightly higher PdI compared to naïve D3-EVs, however, the DNA-EVs derived from RAW 264.7 cells seemed to have larger vesicular sizes as well as showed a heterogeneous sample with a greater PdI, compared to naïve RAW-EVs. The noted changes in the particle diameters of RAW-EVs may be reflective of the exogenous DNA loading. Therefore, we conclude that the subtle differences in physicochemical characteristics of the DNA-loaded EVs are likely not a reason for the observed differences in transfection between the D3- vs. RAW-derived EVs.

Table 2. Effective particle diameters (D_{eff}) of DNA-EVs

Sample	Average D_{eff} (nm)	PdI	Sample	Average D_{eff} (nm)	PdI
Naïve D3-EXO	159.4 ± 42.5	0.4 ± 0.1			
D3-Luc0-EXO	133.7 ± 19.7	0.4 ± 0.1	D3-GFP0-EXO	156.6 ± 7.3	0.4 ± 0.0
D3-Luc0.5-EXO	111.1 ± 5.7	0.4 ± 0.1	D3-GFP0.5-EXO	122.2 ± 5.8	0.5 ± 0.0
D3-Luc1.0-EXO	133.4 ± 25.4	0.3 ± 0.1	D3-GFP1.0-EXO	118.8 ± 0.8	0.4 ± 0.1
D3-MV	216.2 ± 37.2	0.3 ± 0.1			
D3-Luc0-MV	190.2 ± 13.8	0.3 ± 0.1	D3-GFP0-MV	339.3 ± 122.3	0.4 ± 0.1
D3-Luc0.5-MV	306.6 ± 105.5	0.4 ± 0.1	D3-GFP0.5-MV	204.3 ± 17.4	0.4 ± 0.0
D3-Luc1.0-MV	368.5 ± 37.9	0.5 ± 0.1	D3-GFP1.0-MV	176.1 ± 22.3	0.4 ± 0.0
RAW-EXO	174.3 ± 9.9	0.6 ± 0.2			
RAW-Luc0-EXO	483.5 ± 120.4	0.6 ± 0.1	RAW-GFP0-EXO	594.7 ± 204.0	0.5 ± 0.1
RAW-Luc0.5-EXO	163.9 ± 25.4	0.6 ± 0.1	RAW-GFP0.5-EXO	385.0 ± 236.2	0.5 ± 0.1
RAW-Luc1.0-EXO	122.0 ± 15.8	0.3 ± 0.0	RAW-GFP1.0-EXO	556.5 ± 303.8	0.6 ± 0.3

Naïve RAW-MV	199.7 ± 13.7	0.3 ± 0.1			
RAW-Luc0-MV	472.1 ± 198.0	0.5 ± 0.2	RAW-GFP0-MV	276.7 ± 37.7	0.5 ± 0.1
RAW-Luc0.5-MV	668.0 ± 210.6	0.6 ± 0.2	RAW-GFP0.5-MV	288.5 ± 23.8	0.4 ± 0.0
RAW-Luc1.0-MV	585.4 ± 37.5	0.6 ± 0.0	RAW-GFP1.0-MV	386.3 ± 61.3	0.5 ± 0.1

3.3. Transfection of DNA-loaded EVs in the recipient hCMEC/D3 endothelial cells

We studied the ability of the engineered EVs to transfer Luc-pDNA into recipient D3 endothelial cells *in vitro*. Recipient hCMEC/D3 cells were transfected using Luc-EVs derived from either hCMEC/D3 endothelial cells or RAW macrophages. Transfection activity of D3-derived Luc-EVs is shown in **Fig. 2c** and RAW-derived EVs is shown in **Fig. 2d**. Homotypic EVs with analogous cell membranes typically show a higher cellular uptake due to self-recognition compared to heterotopic EVs [76]. Interestingly, as previously noted by us [32], the RAW 264.7 cell-derived EVs showed greater transfection than that of the hCMEC/D3 cell-derived EVs. The RAW-derived DNA EVs continued to show an increase in transfection of Luc-pDNA until 72 h-post-transfection in contrast to the D3-derived EVs that showed no increases in transfection over time. Overall, these results confirmed our previous observations on the limited transfection activity of these carriers [32].

Delivery of pDNA into a cell is a multistep process wherein the DNA cargo must overcome multiple subcellular barriers for successful nuclear entry [77]. The pDNA should be protected from nuclease degradation, undergo cellular uptake, escape the acidic endolysosomes, and the cytosolic release of pDNA is a prerequisite for subsequent nuclear entry. Most non-viral nanoformulations

are relatively more successful in delivering pDNA to actively dividing cells where the nuclear membrane breaks down during mitosis [78] rather than quiescent cells because the large pDNA cannot passively cross the intact nuclear membrane [79]. Additionally, the rate of plasmid entry must be sufficiently high for nuclear entry to overcome the fast degradation of plasmids by cytosolic nucleases following its release from the carrier. hCMEC/D3 are slow-dividing cells with a doubling time of 24 h compared to the 15 h reported for RAW macrophage cells [58] and the confluent endothelial monolayers exhibit contact-inhibition with lower endocytic and pinocytotic transport [80]. Activated immune cells like macrophages can infiltrate through the BBB and have a high potential to adhere to the blood vessel endothelium [81]. EVs especially EXOs isolated from naïve macrophages can bind to the intercellular adhesion molecule and lymphocyte function-associated antigen 1 expressed on BBB endothelial cells [82]. They can also bind to the carbohydrate-binding C-type lectin receptors mediating enhanced interaction and uptake of EXOs into the brain endothelial cells and can enter the brain parenchyma [82, 83]. The various integrins and tetraspanins on the EXOs may also explain the increased uptake of EVs derived from RAW macrophages into the recipient brain endothelial cells [84]. Additionally, EXO membrane proteins like CD9 promote direct fusion of integrins and tetraspanins-rich EXOs and recipient cells. These interactions have also been reported to bypass the endolysosomal pathway permitting direct, cytosolic delivery of the EXOs [85]. As a result, EXO may have shown greater levels of gene expression compared to the MVs. Interestingly, the gene expression of EXOs varied with the type of cell source. RAW-derived EXOs had higher expression than those derived from hCMEC/D3 endothelial cells (**Figs. 2c and 2d**). In comparison to the EVs, the positive control group transfected with Lipofectamine-Luc-pDNA complexes containing an equivalent amount of pDNA showed comparatively higher expression of luciferase (almost 6 to 8-fold increase in luciferase

expression compared to untreated cells) and such increases persisted for over 72 h in hCMEC/D3 endothelial cells (**Fig. 2e**). Our findings are consistent with a previous study that reported that cationic lipids showed an increased photon flux on the 2^{nd-}day post-transfection that decreased gradually over 7 days [86].

Overall, our results on DNA loading into the EVs and the transfection profiles of the DNA-EVs were consistent with our previous study. This suggested that any unintentional/operator-induced biases did cause the higher DNA loading to the smaller EXOs compared to the larger MVs, observations that are in contrast previously published results [30]. Our results also confirmed our previous findings on the slightly greater transfection of the heterotypic, macrophage-derived EVs, compared to the homotypic-, BEC-derived EVs in the recipient BECs. We conducted proteomics analyses of the EVs in an effort to understand this phenomenon.

3.4. Proteomics study to determine potential compositional differences in D3- vs. RAW-derived EVs and their possible effects on the resulting transfection of the DNA-EVs

Biogenesis of EXOs and MVs involves the packaging of cytoplasmic proteins and membrane proteins in the vesicles. Liquid chromatography-tandem mass spectrometry (LC-MS/MS) was used to qualitatively study the proteins present in EVs. Previous studies have identified 295 proteins in urinary exosomes [87] and 272 in mast cell-derived EXOs [88] upon mapping to Entrez gene identifiers. The proteome profiles of our D3-EVs and RAW-EVs resulted in the identification of 136 proteins in D3-EXOs, 116 proteins in D3-MV, 169 proteins in RAW-EXO, and 141 proteins in RAW-MVs. We compared and studied the overlap of our EV proteins with ‘Vesiclepedia’, a publicly available extracellular vesicle protein database. We identified most of the top 100 proteins

enlisted in the Vesiclepedia database (**Table S1**). Following that analysis, we shortlisted key proteins associated with the pathways involved in the cellular uptake and subcellular routing of DNA-EVs (**Table 3**) assuming that these carriers follow a subcellular itinerary similar to synthetic DNA nanocarriers such as lipoplexes and polyplexes [79, 89, 90]. The presence of multiple proteins involved in the binding of EVs to the recipient cells and cellular uptake suggests that multiple pathways including clathrin-mediated endocytosis, phagocytosis, or lipid-raft mediated internalization are likely involved in the internalization of EVs. Similar observations were seen with exosomes derived from immune or tumor cells [82, 91].

Table S1: Top 100 proteins identified in the isolated EVs compared to Vesiclepedia database (*appended to this file*)

Table 3: Proteomic analysis highlighting key proteins related to the transfection of DNA-EVs (*Yes/not detected indicates the expression of the listed proteins in the respective samples).

	Protein Category	**D3-EXO**	**D3-MV**	**RAW-EXO**	**RAW-MV**
1	***Cellular uptake***				
	Clathrin protein	Yes	Yes	Yes	Yes
	Lipid raft - Annexins	Yes	Yes	Yes	Yes
	Phagocytic uptake - Actin	Yes	Yes	Yes	Yes
2	***Cytoplasm to Nucleus transit***				
	Nuclear pore proteins (nucleolin)	Yes	Yes	Not detected	Not detected
	Lamins	Not detected	Not detected	Yes	Yes
	Tubulins	Yes	Yes	Yes	Yes

	Tubulin specific chaperones	Not detected	Not detected	Yes	Yes
	Protein kinesin-1	Not detected	Not detected	Yes	Yes
	Dynactin	Not detected	Not detected	Yes	Yes
3	***Heat shock proteins and chaperones***				
	HSP 90	Yes	Yes	Yes	Yes
	Hspa5	Not detected	Not detected	Yes	Yes
	Heat shock 70 kDa protein	Yes	Yes	Yes	Yes
	HSPβ1	Yes	Yes	Not detected	Not detected
	Heat shock protein 105 kDa	Not detected	Not detected	Yes	Yes
	Hspa8	Not detected	Not detected	Yes	Yes
	T-complex protein 1	Yes	Yes	Yes	Yes

Cytoskeletal elements, tubulin, phospholipids, and lamins assist in the transportation of the EVs towards the nucleus. The presence of laminin receptor B2CY77 in RAW-EV indicates the presence of lamin, an important component of the nuclear envelope, in these EVs. Further, the presence of tubulin family of proteins (TBB5β, TBB4β, and TBB6β in D3-EVs and TBA1Cα in RAW-EV), and tubulin-specific chaperones (TBCD in RAW-EVs) suggests that the late endosomes can be transported towards to the nuclear envelope. Interaction of protein kinesin-1 (KINH in RAW-EVs) with dynactin subunit (D3YX34 specifically in RAW-EXO) which binds to the dynein heavy chain may traffic the late endosomes containing EVs towards the nuclear envelope via microtubule transport. Proteins such as the tubulin-specific chaperones, protein kinesin-1, dynactin, and laminin receptor seem to be preferentially expressed in RAW-EVs, and that too, specifically in RAW-EXOs. Therefore, the selective enrichment of the above-mentioned proteins in RAW-EXOs likely contributed to the measurable transfection of Luc-pDNA compared to the other EVs due to effective routing of the RAW-EXOs to the nucleus (**Fig. 2c, d**).

We speculate that the enrichment of HSP proteins in the EVs may have contributed to the observed ATP increases in the normoxic as well as hypoxic endothelial cultures.[92]. Heat-shock 70-kDa proteins (HSP70, HSP71A), constitutive heat-shock proteins (HSPA8 and HSPA5), HSP105, and HSP90 (HSP90A/B) were present in EXOs and MVs isolated from hCMEC/D3 and RAW 264.7 cells. HSP-beta (HSPβ1) was specifically expressed in D3-EVs, while HSP105 and HSPA8 (Q3UBA6) were specifically observed in RAW-EVs. HSPA8 and HSP90 are reported to be among the top ten proteins found in most of the EXOs [93].

3.5. Mitochondrial transfer from EVs to recipient brain endothelial cells

EVs are reported to contain mitochondria, mitochondrial proteins, or mitochondrial DNA (mtDNA) and are transferable between cells [34]. Transfer of mitochondria either in the form of depolarized mitochondria that is known to be present in MVs [34] or as polarized mitochondria in EXOs [35] have been reported. Mitochondrial proteins like ATP5A were enriched in the MVs derived from brain endothelial cells [32, 94] and the umbilical cords of infants [95]. Moreover, the presence of ATP5A is also reported in the exosomal fraction isolated from murine cancer-associated fibroblasts and in serum obtained from adults with Parkinson's disease [96, 97]. EXOs are also reported to contain mtDNA [270].

Transfer of mitochondria to the recipient cells is possible via either formation of tunnelling nanotubes, cellular fusion, GAP junctions, or microvesicles [98, 99]. F-actin microtubules or tunnelling tubes facilitate the transfer of cytoplasmic content and mitochondria to the recipient cells [100]. Mitochondrial transfer to cells via EVs can thus increase the cellular bioenergetics in

the recipient cells [34, 35]. It had been reported that that stem cells or stem cell-derived EVs decrease inflammatory responses with improved regeneration, and repair injury ranging from immediate areas to remote areas in both *in vitro* and *in vivo* models of wound healing [101, 102]. The secretion of paracrine factors, transfer of mitochondria [98, 99] or the presence of protective/antiapoptotic genetic messages or macrophage polarizing miRNAs [103, 104] are known to revive the injured cells and protect against subsequent tissue injury.

Phinney *et al*. reported that MV-mediated mitochondrial transfer under oxidative stress can improve the cell survival in the recipient macrophages cells by improving their mitochondrial bioenergetics. The authors reported that though EXOs do not contain mitochondria, they contain mtDNA that can be also transferred to the recipient cells [34]. Despite the low transfection activity of EVs containing exogenous DNA, we wanted to determine if mitochondria in EVs can be exploited for increasing the cellular energetics in the recipient endothelial cells. During ischemia/reperfusion (I/R) injury, the oxygen-glucose deprived endothelial cells lining the BBB undergo structural and functional damage leading to poor patient outcomes post-I/R injury [14]. Therefore, protection of the BBB endothelial cells is considered an effective strategy to decrease acute cell death in ischemic stroke. The presence of mitochondria organelles can increase the intracellular ATP levels and cell viability of the injured endothelial cells. Improving the mitochondrial bioenergetics contribute to neuroprotection in an ischemic brain and repair brain injury [105]. The lack of ATP synthesis following oxygen and glucose deprivation sets off energy failure and loss of ionic gradients [106]. Albeit the lack of ATP cannot be equated with ischemic cell death, it is important to note that the initial trigger of ATP loss orchestrates multiple ionic, biochemical, and cellular events that lead to tissue death [107]. It is also known that glutamate

excitotoxicity and calcium overload serve as additional triggers of cell death resulting in further depletion of ATP that compounds the events leading to acute cell death. Therefore, we posit that mitochondrial-transfer mediated ATP increases may serve to decrease the endothelial cell death in an *in vitro* oxygen-glucose deprivation model of stroke.

MitoTracker Deep Red (MitoT) is a carbocyanine dye that stains respiring mitochondria in live cells [108, 109] utilizing the mitochondrial membrane potential. We pre-labelled mitochondria in hCMEC/D3 and RAW 264.7 cells using MitoT and isolated EXOs and MVs (D3-MitoT-EXO, D3-MitoT-MV, RAW-MitoT-EXO, and RAW-MitoT-MV) to evaluate if the labelled mitochondria can be transferred to recipient hCMEC/D3 endothelial cells. Brain endothelial cells were treated with varying amounts of labelled EVs at doses ranging from 3 – 600 μg total EV protein. At a low dose of 3 μg EV protein, D3-MitoT-EXO showed no MitoT positive signals up to 72 h whereas D3-MitoT-MV showed punctate fluorescence at 48 h of post-incubation (**Fig. 3a-c**). Furthermore, we noticed increased intracellular puncta in D3-MitoT-MV-treated cells with EV protein content ranging from 3 to 24 μg as the incubation times increased from 24 – 72 h. Cells dosed with D3-MitoT-MV from 100 μg up to 600 μg showed punctate signals at all observed time points (24-72 h). However, the signals were visible in the case of D3-MitoT-EXO only at the 100 μg protein dose at 24 h with prominent signals noted at 48 h and 72 as well. Nevertheless, there were differences in the nature of the staining observed with D3-MitoT-EXO and D3-MitoT-MV-treated cells. D3-MitoT-EXO showed faint staining at an exposure time of 200 ms despite the higher dose of 100 μg, whereas the staining was brighter in cells treated with D3-MitoT-MV even at a lower exposure time of 70 ms. The intensity of fluorescent signals was found to be dependent on the EV protein dose and incubation times.

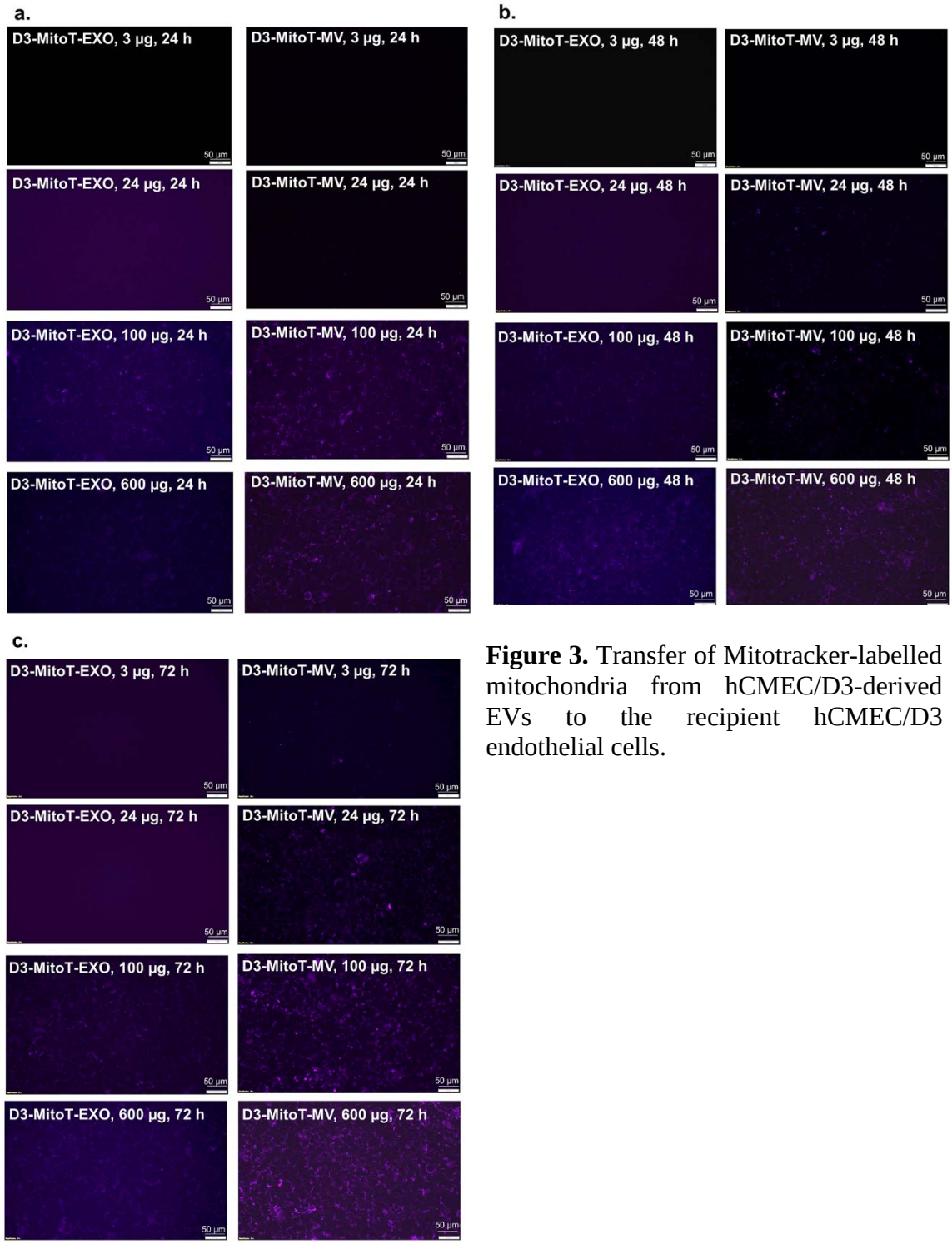

Figure 3. Transfer of Mitotracker-labelled mitochondria from hCMEC/D3-derived EVs to the recipient hCMEC/D3 endothelial cells.

We noted similar observations for RAW-MitoT-EXO and RAW-MitoT-MV at higher EV protein doses as well as at increasing incubation times from 24 to 72 h (**Fig**. **S3**). Yet another striking feature was the fact that both microvesicles: D3-MitoT-MV and RAW-MitoT-MV, showed fluorescent signals at lower treatment doses within 24 h compared to the exosomes: D3-MitoT-EXO and RAW-MitoT-EXO, that required a higher amount of protein and increased amounts of incubation time for detecting MitoT fluorescent signals. However, comparing the signal intensities, the appearance of fluorescent signals in cells was relatively earlier and more discrete with homotypic D3-MitoT-MV at lower protein contents than those incubated with the heterotypic RAW-MitoT-MV which showed fluorescent signals later and at longer exposure times. For instance, cells treated with 100 μg of D3-MitoT-MV showed higher cellular uptake than those treated with 100 μg of RAW-MitoT-MV 24-, 48-, and 72 h post-incubation. This underscores the fact that despite the low transfection of the homotypic D3-derived-EVs, these BEC-derived EVs are potent carriers for mitochondrial transfer. To summarize, EXOs and MVs derived from MitoT-labelled cells demonstrated a significant accumulation of mitochondria in the recipient hCMEC/D3 endothelial cells.

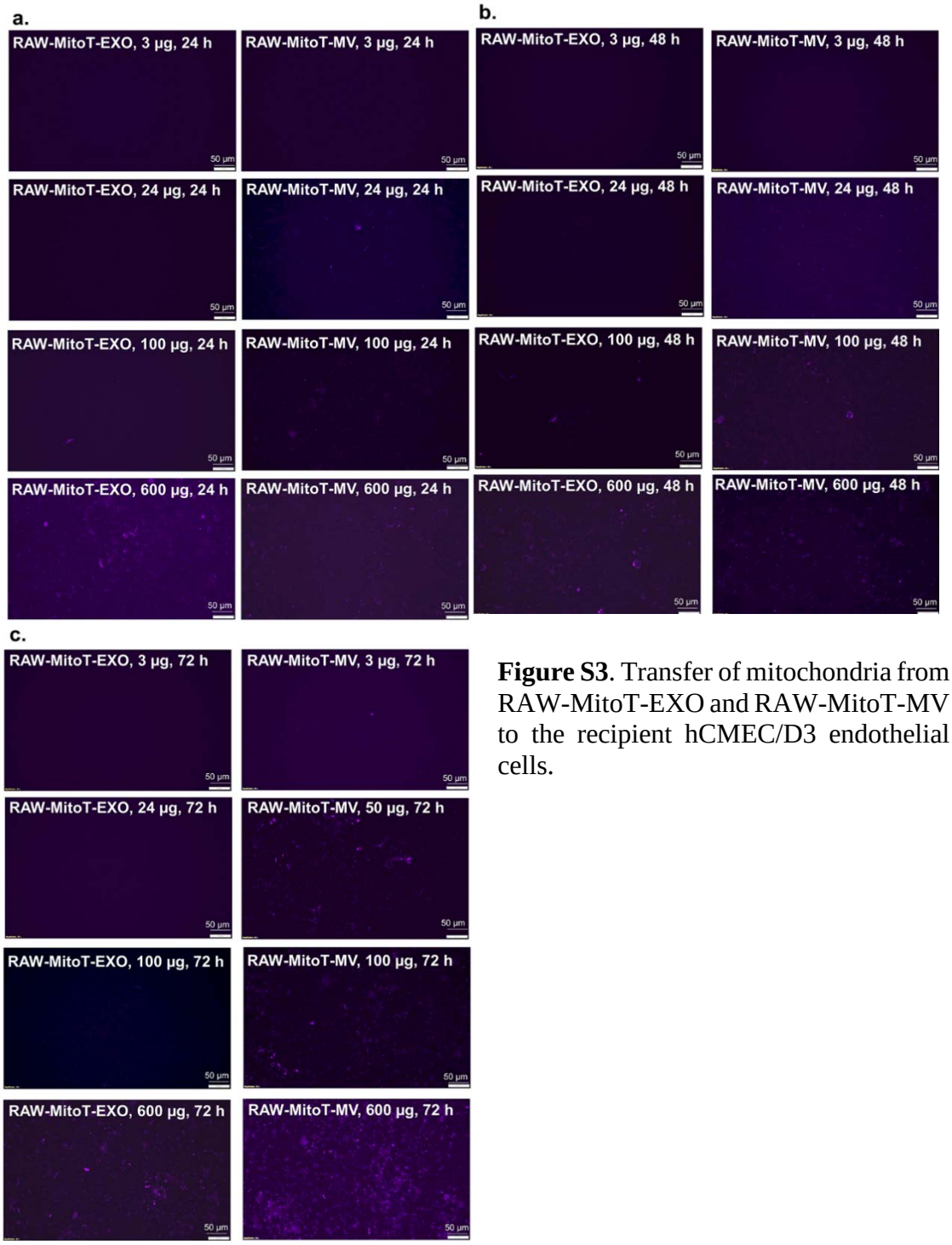

Figure S3. Transfer of mitochondria from RAW-MitoT-EXO and RAW-MitoT-MV to the recipient hCMEC/D3 endothelial cells.

We noticed that MVs were more efficient in transferring mitochondria compared to EXOs, as noted by the brighter fluorescent puncta in the MV-treated cells and that aligned well with the fact that MVs incorporate mitochondria during their biogenesis. It is known that mitochondria undergo a series of dynamic changes, including biogenesis, shape changes and selective degradation and

rapid transport along with cell bodies to extremities [110]. It may well be possible that these MV mitochondria are functional with their full complement of proteins, lipids, and mitochondrial DNA. Although MV-associated mitochondria have also been previously reported [34], recent reports have demonstrated the presence of mitochondria in exosomes as well [35]. EXOs derived from airway myeloid-derived regulatory cells from both healthy and asthmatic subjects transferred mitochondria to T cells and co-localized with the mitochondrial network and regulated bioenergetics in the recipient T cells [35]. Panfoli *et al.* demonstrated that the EXOs isolated from new-born infants can produce ATP and consume oxygen with the presence of electrochemical membrane potential similar to isolated mitochondria [111]. Some mitochondrial proteins such as voltage-dependent anion channel 1 (VDAC1) and adenosine triphosphate synthase subunit alpha (ATP5A) were also detected in the exosomal fraction isolated from murine cancer-associated fibroblasts and in the serum obtained from adults with Parkinson's disease isolated at 100,000*x*g and tested positive for proteins of endocytic origin [96, 97]. Some studies evaluated the entire supernatant fraction of conditioned media or plasma after removal of apoptotic bodies for MV studies [112, 113]. Zhang *et al.* used the EVs isolated from plasma deprived of cell debris and apoptotic bodies to study the mitochondrial activity. The authors found that the all fractions of EVs contained respiring mitochondria, with the highest (99.98%) being in the large-sized EVs (1 – 6 μm), intermediate (95.91%) in EVs sized 100 nm – 1 μm and low (62.72%) in small-sized EVs < 100 nm [113]. In summary, our results align well with previously reported observations that both the EXO and MV fractions contain active, healthy and functional mitochondria.

3.6. Uptake of MitoT-EVs by cortical and granule neurons in brain slices from mice

Cortical slices obtained from non-surgical control mice were incubated in D3-MitoT-EVs for 2 h at 37 °C. We observed punctate intracellular staining suggesting the EV-mediated transfer of polarized mitochondria to the cortical (**Fig. 4a**) and hippocampal (dentate gyrus, **Fig. 4b**) slices, whereas the untreated cortical slices showed notably less staining in both regions (**Fig. 4a&b**). These results suggest that EVs can transfer polarized mitochondria to neuronal cells in cortical and hippocampal brain slices. The brain slices incubated with D3-MitoT-MV exhibited less of the same punctate intracellular staining as the D3-MitoT-EXO treated slices in both the hippocampal and cortical slices, albeit slightly more staining than the untreated control slices. Although these images were obtained from healthy mice, the potential of using EV and MVs to increase cellular energy levels in injured neurons is intriguing and has significant implications in treating ischemic injury *in vivo*. Neurons can a be injured due to oxidative stress and inflammation as a result of cell death following ischemia reperfusion injury. A recent report demonstrated that mitochondrial transfer from mesenchymal stem cells co-cultured with mice primary neurons rescued the H_2O_2-injured neurons and improved metabolism [114]. Seahorse analysis revealed that the mitochondrial respiratory parameters such as basal respiratory rate, spare respiratory capacity, ATP production and proton leak in the injured neurons were significantly improved upon mitochondrial transfer [114]. Impaired and depolarized mitochondria result in decreased ATP, increased reactive oxygen species and calcium overloading which opens up the membrane permeability transition pore releasing cytochrome C, eventually leading to apoptotic death. Mitochondrial fusion with the

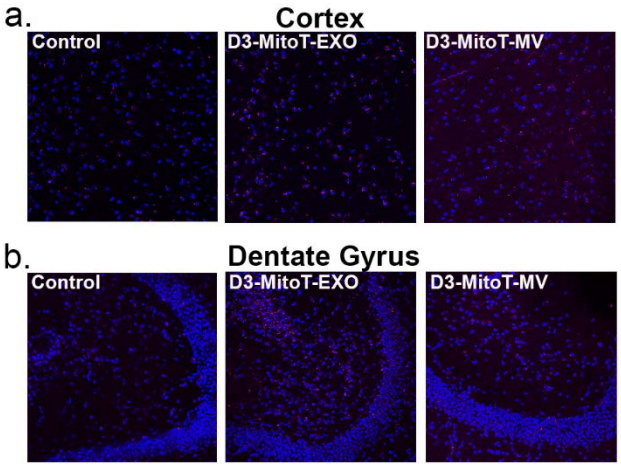

Figure 4. Uptake of MitoT-EVs by neurons in mice acute brain slices.

injured cells causes rapid exchange of mitochondrial DNA, mitochondrial membranes and mitochondrial metabolites within mitochondrial network and repair the damaged ones. Thus, mitochondrial transfer increases the chances of neuronal cell survival upon ischemic attack.

3.7. Effect of EV delivery on the ATP levels in the ischemic endothelial cells

It has been reported that depolarized mitochondria were transferred from the mesenchymal stem cells to macrophages via MVs and that these mitochondria were repurposed by undergoing fusion with the mitochondrial network of macrophages and improved their bioenergetics [34]. Thus, it is reasonable to expect that the positive effects of mitochondria-induced increases in bioenergetics would be more pronounced in ischemic cells that have impaired mitochondrial function. Therefore, we determined the effects of transferring naïve EVs in brain endothelial cells subjected to an ischemic attack using an *in vitro* oxygen-glucose deprivation (OGD) model of stroke. We used a CellTiter Glo-Luminescent Cell Viability assay (referred to as "ATP assay" henceforth) to measure the resulting ATP levels upon EV exposure. We chose the ATP assay to determine the effects of EV exposure as it is a rapid and sensitive technique for evaluating the cell viability of the treated cells [115, 116] and the ATP readout is directly proportional to the number of cells in culture [117]. The cytoplasmic mitochondrial volume of rat brain endothelial cells was almost two to four-fold higher compared to the other non-brain endothelial cells (2 to 5%), suggesting that the brain endothelial cells have a higher metabolic activity [50]. Additionally, hypoxic conditions lead to disruption of tight junctions and apoptosis in BECs further increasing the need for mitochondrial metabolism for endothelial survival [51]. Oxygen-glucose deprivation reduces oxidative phosphorylation and induces energy failure [34]. Recovery of bioenergetics in cells is indicated by their ability to generate mitochondrial ATP in coupled with proton leak and/or

generation of reactive oxygen species [34]. We first optimized the exposure time of cells to determine the reproducibility of simulating OGD-induced cell death in the hCMEC/D3 brain endothelial cells. We determined that a 4 h OGD exposure was sufficient to mediate at least 50% cell death as measured using the ATP assay (**Fig. S4**).

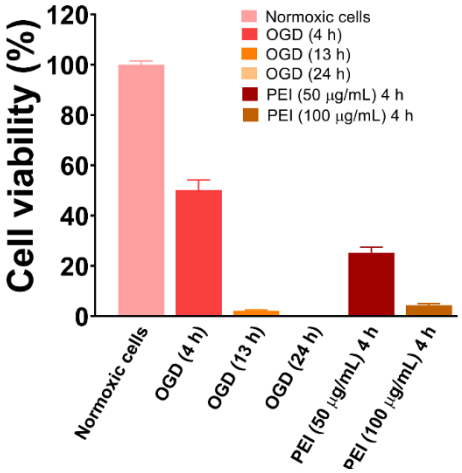

Figure S4. Modelling OGD-induced cell death in hCMEC/D3 monolayers.

We first exposed healthy hCMEC/D3 endothelial cells (cultured under normoxic conditions) to different EV protein doses ranging from 14.6 to 174.5 μg (per 0.32 cm^2/well in a 96-well plate). These selected doses were equivalent to 50, 100, 200, 400 and 600 μg per 0.85 cm^2 area of 48-well plate that was previously used in the MitoT-EV study (**Fig. 3 and Fig. S3**). Seventy-two h post-incubation with normoxic monolayers, no significant differences were found in the ATP levels (and the resulting cell viabilities) in cells that were treated with both D3- and RAW-EXOs and D3-MV groups at 14.6 and 29.1 μg and compared to the untreated cells (**Fig. 5a**). The cell viabilities however decreased with an increase in the treatment dose of EXO dose from 58.2 to 174.5 μg and the case of D3-MVs, from 29.1 μg and upward. A previous study reported no cytotoxicity of milk-derived EVs up to doses of 200 μg protein/mL in Caco-2 intestinal monolayers since these cells naturally absorb digestive products [118]. Hansen *et al*. observed decreased Caco-2 cell viability when treated with 50 μg/mL of Alexa

Fluor-labelled EVs isolated from milk after 6 h but the cell viability was regained after 24 h, which however were not confirmed in the successive experiments performed by the group [119].

However, under OGD conditions that simulate ischemic injury, all types of EVs regardless of parent cell source resulted in increased cellular ATP levels relative to control, untreated hypoxic cells (**Fig. 5b**). The increased relative ATP levels were likely indicative of cell survival effects at all tested EVs doses. The cell viability was significantly higher in recipient cells when incubated with all doses of the different EVs compared to the control group. Incubation of OGD-exposed endothelial cells with D3- and RAW-EVs increased the ATP levels by nearly 100 to 200-fold as a function of the EV protein dose. At the same time, no differences were found when the recipient cells were treated with D3-EXO and D3-MV. However, the ATP levels of D3-EVs post-incubation were higher than the ATP levels of RAW-EVs post-incubation (**Fig. 5b and 5c**). Our results showed that at least 14.6 µg of total EV protein is required to increase the cellular ATP levels. A similar observation was noted when EVs derived from human Wharton's jelly

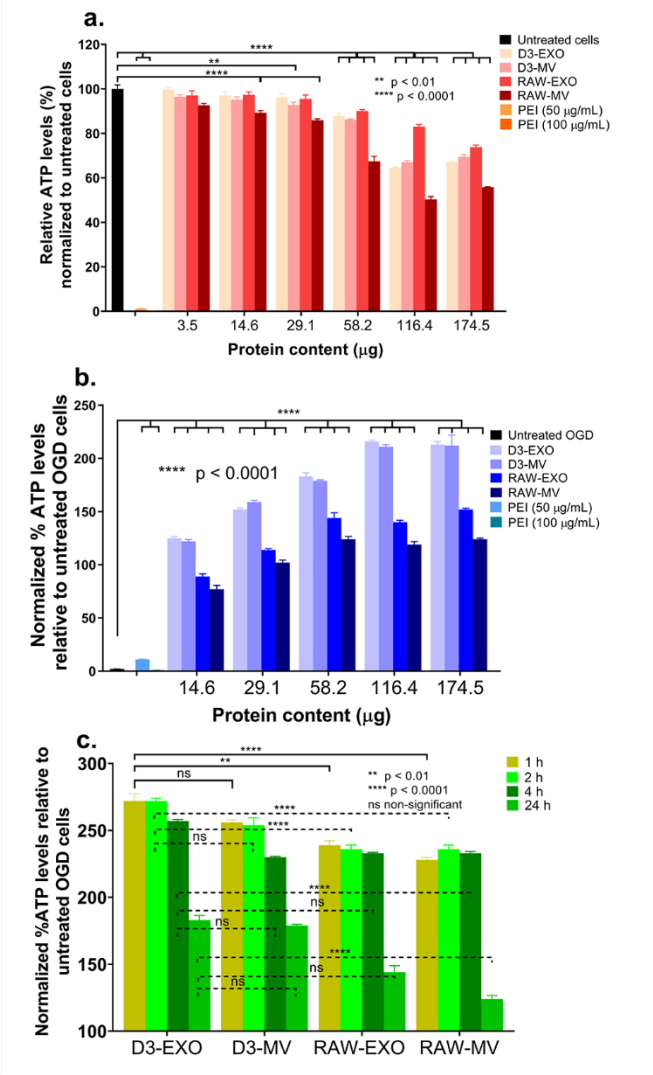

Figure 5. Effects of EV exposure on the cell viability of hCMEC/D3 endothelial cells under normoxic and hypoxic (OGD) conditions.

mesenchymal stem cells were used to treat OGD-exposed mouse neuroblastoma cells [120]. Another study [121] reported that EV doses of 200 μg yielded the maximum cell proliferation, while 50 μg of EVs was the minimal effective dose to increase cell proliferation in neural stem cells under OGD conditions. Our results further confirmed that EVs can increase cellular ATP levels in a dose-dependent manner. A modest increase in cell viability was observed at the highest protein dose of 116.4 μg with D3-derived EVs and at doses greater than 58.2 μg with RAW-derived EVs. It is likely that at the higher doses, the cells may have shown a reduced uptake with time causing the observed plateau effects. A saturation in uptake or intake equivalent to intracellular processing of EVs has been reported after 18 h [119] especially in the case of milk-derived EVs [122]. Saari *et al*. had similar observations with paclitaxel-loaded EVs which showed increased toxicity with an increase in concentrations in LNCaP and PC-3 cell lines and their respective EVs. However, after incubating cells with 10^9 paclitaxel loaded-EVs/mL, a saturation point with maximum cytotoxic effect was reached at 24 h [123]. Meanwhile, HEK293T-derived EVs showed early uptake within 2 h with a peak at 12 h and then decreased up to 24 h. The lower values may also be due to the exocytosis of EVs after 24 h [122].

The protective effects of the EVs appeared to reach their maximum at about 2 h post-incubation (**Fig. 5c**) in hypoxic cultures. As described in the above paragraph, EV uptake also shows a saturation and a time-dependent uptake. Hansen *et al.* observed a plateau in EV uptake 18 h post-exposure [119]. The saturation effects are likely due to the active, energy-dependent endocytic uptake of EVs [91, 124, 125] and not via passive membrane fusion, which caused an inhibition in the uptake of EVs [126]. The resulting ATP levels were consistently higher with D3-derived EVs compared to the RAW-derived EVs suggesting that under cell duress, the recipient D3 brain

endothelial cells preferentially internalized the homotypic D3-derived EVs as opposed to the heterotypic RAW macrophage-derived EVs (**Fig. 5b**).

ATP is the most common intracellular energy source and importantly, in high energy consuming-tissues like the heart and brain, mitochondria produce 80-90% of the cell's ATP [127]. Depletion of ATP levels is thought to prevent efficient post-ischemic repair [127]. The EV-mediated ATP increases suggest that this may be a promising approach to decrease acute cell death and activate ischemic repair pathways to limit post-stroke damage. Mitochondrial transfer helps to rescue metabolism and protects the neurons and other brain cells from tissue injury. Brain endothelial cells also take up extracellular mitochondria derived from endothelial progenitor cells under OGD conditions [128]. EXOs are also reported to contain mitochondria or mtDNA which can be transferred across distant cells [34, 35, 47, 48, 111, 129]. Mitochondrial DNA and intracellular ATP were upregulated in the oxygen-glucose deprived endothelial progenitor cells when treated with endothelial progenitor cell-derived mitochondria [128]. Mitochondrial DNA can also be imported into mitochondria irrespective of the mitochondrial membrane potential [130]. The mammalian mtDNA is essential to couple respiration to ATP synthesis and oxidative photophosphorylation [131]. It also encodes functional RNAs in intramitochondrial translation. Transfer of mtDNA can be of crucial significance in increasing the mitochondrial load in the recipient cells. The mtDNA can be imported into the mitochondria once it reaches the cytosol of the recipient cell [129]. EVs derived from cardiomyocytes containing chromosomal DNA were transferred to the nuclei or cytosol of the recipient fibroblasts [132]. Transfer of intact/full mitochondria can also import mtDNA and provide a template for synthesis of DNA and RNA [130]. Adipose stem cell-derived EXOs reverted mitochondrial dysfunction by contributing

complex 1 to the electron transfer system and coupling efficiency as well as by restoring mitochondrial membrane potential [133]. Mesenchymal stem cell-derived EXO containing glycolytic enzymes restored the glycolysis and ATP levels with reduced oxidative stress in mice subjected to 30 min of ischemia followed by reperfusion [134] and also increased the levels of extracellular ATP [135]. Our data and these findings thus suggest that EVs-derived from D3 endothelial and RAW cells may increase the cellular bioenergetics of brain endothelial cells in an animal model of ischemic stroke through mitochondrial transfer, providing an extracellular source of glycolytic enzymes and/or the transfer of mtDNA.

3.8. Delivery of ATP5A protein via EV/ATP5A complexes to OGD-exposed BECs

It is noteworthy that D3-derived microvesicles were highly enriched in ATP5A1 [32, 94], a subunit of the mitochondrial ATP synthase protein that catalyzes ATP synthesis [136]. From an engineering perspective, we tested if we could load exogenous ATP5A into EVs to further buttress its capability to deliver ATP5A protein. ATP5A1 is a mitochondrial [137], nucleus-encoded protein [138] biosynthesized by the mitochondria to produce ATP from ADP in presence of a proton gradient. Reduced supply of blood and oxygen during ischemia causes an imbalance of the energy production and depletes the high energy phosphates, ATP. Intracellular delivery of ATP increases the chemical energy which can be used for the various cellular process such as exocytosis, endocytosis, metabolism, apoptosis, regulate innate immunity, cell differentiation, cell reprogramming, etc. [139]. Direct infusion of exogenous ATP is not possible due to its anionic charge and hydrophilic nature which forbids delivery through the cellular membrane. Moreover, the systemic half-life of ATP is short (< 40s) due to degradation by ectonucleotidases [140].

Hypoxia/reperfusion of cells decreases the ATP5A/ mitochondrial-encoded protein cytochrome-c oxidase I ratio [138] and ATP5A mRNA levels [141] further exacerbating ischemic injury.

ATP5A is a large cationic protein (MW 59.8 kD, pI 9.2) that cannot diffuse or penetrate through the cell membrane. ATP5A contains 68 cationic residues (arginine and lysine) at a physiological pH of 7.4 that can form a complex with the negatively-charged EV membranes via electrostatic interactions. The formation of the EV/ATP5A complexes was confirmed using a native polyacrylamide gel (**Fig. 6a**). Coomassie dye stained both the ATP5A and EV proteins. Under native PAGE conditions, ATP5A is slightly positively charged at the running buffer pH of 8.3. On the other hand, the negatively-charged EVs ranging with a surface zeta potential of -4 and -12 mV (**Fig. 6a**) will migrate towards the anode. While the cationic free ATP5A protein stayed at the loading point, EV protein: ATP5A complexes at a weight/weight ratio (w/w) of 5:1 resulted in the retention of the formed complexes at the loading point while the excess free EVs slightly migrated towards the anode (+) confirming the neutralization of protein charges by EV membranes. It should be noted that this pattern of migration of EV/protein complexes was consistent with previously reported findings on EV complexes with a similar cationic protein, brain-derived neurotrophic factor [82].

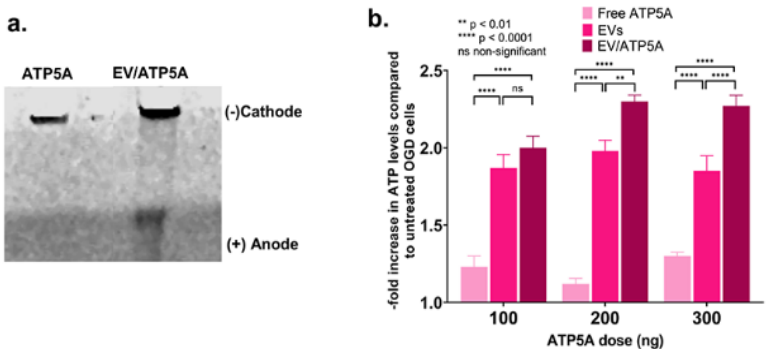

Figure 6. Formation of EV/ATP5A complexes confirmed using native gel electrophoresis (a). Effect of ATP5A/EV complexes on ischemic endothelial cells (b).

The effect of EV/ATP5A complexes on the resulting ATP levels in OGD-exposed hCMEC/D3 is shown in **Fig. 6b**. Incubation of free ATP5A1 with endothelial cells exposed to OGD increased the cellular ATP levels. However, increasing the dose of free ATP5A1 from 100 to 300 ng did not result in a significant increase in the ATP levels that almost remained constant ($p > 0.05$) regardless of the ATP5A dose. As observed and discussed in section 3.7, naïve EVs increased the ATP levels of the endothelial cells exposed to OGD. However, the increase in the ATP levels is not significant ($p > 0.05$) with an increase in the naïve EV doses (500, 1000 and 1500 ng) added in amounts equivalent to those in EV/ATP5A complexes. The EV/ATP5A complexes containing 100 ng of ATP5A also did not result in a significant increase in the ATP levels compared to cells treated with naïve EVs. However, the ATP levels increased significantly ($p=0.0097$) in cells treated with EV/ATP5A complexes containing 200 ng of ATP5A protein. A further increase in the ATP5A dose to 300 ng in the EV/ATP5A complexes showed elevated ATP levels ($p=0.02$). Our observations point at a trend that higher ATP5A protein doses (200 and 300 ng) delivered via EVs increased ATP levels by ca. 2.3-fold compared to about 1.9-fold in the case of naïve EVs.

4. Conclusions

We suggest that the natural overlap of exosomal biogenesis and the intracellular trafficking pathways of DNA-EVs may explain the greater DNA loading in smaller EXOs compared to the larger MVs, in contrast to results published in a previous report [30]. Our EV proteomic analysis revealed that the macrophage-derived EXOs are preferentially enriched with proteins that participate in the trafficking of EXOs towards the nucleus and we suggest that this is a likely reason for the higher transfection of the macrophage-derived EXOs compared to the other tested carriers. We have demonstrated, for the first time, that homotypic, endothelial-derived EVs, result in a

greater extent of mitochondrial transfer to the recipient's brain endothelial cells and resulting ATP increases, compared to heterotypic, macrophage-derived EVs. We have also demonstrated EV-mediated mitochondrial transfer to acute brain cortical and hippocampal slices. We further demonstrated that the endothelial-EVs can deliver exogenous ATP5A, a mitochondrial protein, to ischemic endothelial monolayers. Our findings suggest that EV carriers have immense potential to increase cellular- and mitochondrial bioenergetics in the endothelial cells lining the BBB and can be developed for the treatment of not only ischemic stroke but also for treating those brain disorders wherein the permeability of BBB is altered.

Conflicts of interest

There are no conflicts of interest to declare.

Funding

This work was supported via start-up funds for the Manickam laboratory from Duquesne University (DU) and a Faculty Development Fund (Office of Research, DU) to the PI. The proteomics study was conducted at the UPMC Hillman Cancer Center Proteomics Facility supported in part by award P30CA047904.

Acknowledgments

The authors are grateful to Dr. Rehana Leak for the inspiring discussions. The authors are thankful to Mr. Tarun Bhatia in the Leak Lab for technical assistance and Dr. Jelena Janjic for allowing the use of Malvern Zetasizer Nano. The authors also appreciate Dr. Lauren O'Donnell, Mss. Manisha Chandwani and Yashika Kamte for assistance with flow cytometry experiments.

The authors are also thankful to the Biological Sciences Department of Duquesne University for equipment support and Biomedical Mass Spectrometry Center, University of Pittsburgh School of Medicine for the proteomics study.

Author Contributions

D.S.: Conceptualization; A.D. and D.S.: methodology, investigation, formal analysis, data collection; A.B., N.Q. and P.H.: Methodology, investigation, and data collection of EV uptake by acute brain slices; W.Z., and K.D. trained A.D. in experimental methods related to EV isolation, characterization, DNA loading and transfection; C.S., and G.S.: experimental assistance; D.S.: resources and supervision, A.D. and D.S. wrote the manuscript.

Appendix A. Supplementary data

Supplementary data related to this article can be found in the accompanying Word file.

Data availability statement: The raw data required to reproduce these findings will be available upon request to the corresponding author.

5. References

[1] Johnson W, Onuma O, Owolabi M, Sachdev S. Stroke: a global response is needed. Bulletin of the World Health Organization. 2016;94:634-A.
[2] CDC. Stroke Facts. National Center for Chronic Disease Prevention and Health Promotion , Division for Heart Disease and Stroke Prevention. 08 September 2020 ed. USA: Centers for Disease Control and Prevention; 2020.
[3] Jiang X, Andjelkovic AV, Zhu L, Yang T, Bennett MVL, Chen J, et al. Blood-brain barrier dysfunction and recovery after ischemic stroke. Prog Neurobiol. 2018;163-164:144-71.
[4] D'Souza A, Dave KM, Stetler RA, Manickam DS. Targeting the blood-brain barrier for the delivery of stroke therapies. Advanced Drug Delivery Reviews. 2021.

[5] Russo E, Nguyen H, Lippert T, Tuazon J, Borlongan CV, Napoli E. Mitochondrial targeting as a novel therapy for stroke. Brain Circ. 2018;4:84-94.
[6] del Zoppo GJ. Stroke and neurovascular protection. N Engl J Med. 2006;354:553-5.
[7] D'Souza A, Dave KM, Stetler RA, S. Manickam D. Targeting the blood-brain barrier for the delivery of stroke therapies. Advanced Drug Delivery Reviews. 2021;171:332-51.
[8] Lo EH, Moskowitz MA, Jacobs TP. Exciting, Radical, Suicidal. Stroke. 2005;36:189-92.
[9] del Zoppo GJ. The neurovascular unit in the setting of stroke. J Intern Med. 2010;267:156-71.
[10] Lo EH. Experimental models, neurovascular mechanisms and translational issues in stroke research. Br J Pharmacol. 2008;153 Suppl 1:S396-S405.
[11] Guo S, Kim WJ, Lok J, Lee S-R, Besancon E, Luo B-H, et al. Neuroprotection via matrix-trophic coupling between cerebral endothelial cells and neurons. Proceedings of the National Academy of Sciences. 2008;105:7582-7.
[12] Wang X, Yu X, Xie C, Tan Z, Tian Q, Zhu D, et al. Rescue of Brain Function Using Tunneling Nanotubes Between Neural Stem Cells and Brain Microvascular Endothelial Cells. Mol Neurobiol. 2016;53:2480-8.
[13] Neuhaus AA, Couch Y, Hadley G, Buchan AM. Neuroprotection in stroke: the importance of collaboration and reproducibility. Brain. 2017;140:2079-92.
[14] Shi Y, Jiang X, Zhang L, Pu H, Hu X, Zhang W, et al. Endothelium-targeted overexpression of heat shock protein 27 ameliorates blood–brain barrier disruption after ischemic brain injury. Proceedings of the National Academy of Sciences. 2017;114:E1243.
[15] O'Brien K, Breyne K, Ughetto S, Laurent LC, Breakefield XO. RNA delivery by extracellular vesicles in mammalian cells and its applications. Nature Reviews Molecular Cell Biology. 2020;21:585-606.
[16] Wu P, Zhang B, Ocansey DKW, Xu W, Qian H. Extracellular vesicles: A bright star of nanomedicine. Biomaterials. 2021;269:120467.
[17] Vader P, Mol EA, Pasterkamp G, Schiffelers RM. Extracellular vesicles for drug delivery. Advanced Drug Delivery Reviews. 2016;106:148-56.
[18] de Jong OG, Kooijmans SAA, Murphy DE, Jiang L, Evers MJW, Sluijter JPG, et al. Drug Delivery with Extracellular Vesicles: From Imagination to Innovation. Accounts of Chemical Research. 2019;52:1761-70.
[19] Elsharkasy OM, Nordin JZ, Hagey DW, de Jong OG, Schiffelers RM, Andaloussi SEL, et al. Extracellular vesicles as drug delivery systems: Why and how? Advanced Drug Delivery Reviews. 2020.
[20] Tang T-T, Wang B, Lv L-L, Liu B-C. Extracellular vesicle-based Nanotherapeutics: Emerging frontiers in anti-inflammatory therapy. Theranostics. 2020;10:8111-29.
[21] Meng W, He C, Hao Y, Wang L, Li L, Zhu G. Prospects and challenges of extracellular vesicle-based drug delivery system: considering cell source. Drug Deliv. 2020;27:585-98.
[22] Busatto S, Pham A, Suh A, Shapiro S, Wolfram J. Organotropic drug delivery: Synthetic nanoparticles and extracellular vesicles. Biomedical microdevices. 2019;21:46.
[23] Walker S, Busatto S, Pham A, Tian M, Suh A, Carson K, et al. Extracellular vesicle-based drug delivery systems for cancer treatment. Theranostics. 2019;9:8001-17.
[24] Alvarez-Erviti L, Seow Y, Yin H, Betts C, Lakhal S, Wood MJ. Delivery of siRNA to the mouse brain by systemic injection of targeted exosomes. Nat Biotechnol. 2011;29:341-5.
[25] Ha D, Yang N, Nadithe V. Exosomes as therapeutic drug carriers and delivery vehicles across biological membranes: current perspectives and future challenges. Acta Pharm Sin B. 2016;6:287-96.

[26] El Andaloussi S, Mäger I, Breakefield XO, Wood MJ. Extracellular vesicles: biology and emerging therapeutic opportunities. Nat Rev Drug Discov. 2013;12:347-57.
[27] Raposo G, Stoorvogel W. Extracellular vesicles: Exosomes, microvesicles, and friends. Journal of Cell Biology. 2013;200:373-83.
[28] Yáñez-Mó M, Siljander PRM, Andreu Z, Zavec AB, Borràs FE, Buzas EI, et al. Biological properties of extracellular vesicles and their physiological functions. Journal of extracellular vesicles. 2015;4:27066-.
[29] van Niel G, D'Angelo G, Raposo G. Shedding light on the cell biology of extracellular vesicles. Nature Reviews Molecular Cell Biology. 2018;19:213-28.
[30] Kanada M, Bachmann MH, Hardy JW, Frimannson DO, Bronsart L, Wang A, et al. Differential fates of biomolecules delivered to target cells via extracellular vesicles. Proceedings of the National Academy of Sciences. 2015;112:E1433.
[31] Lamichhane TN, Raiker RS, Jay SM. Exogenous DNA Loading into Extracellular Vesicles via Electroporation is Size-Dependent and Enables Limited Gene Delivery. Molecular Pharmaceutics. 2015;12:3650-7.
[32] Dave KM, Zhao W, Hoover C, D'Souza A, D SM. Extracellular Vesicles Derived from a Human Brain Endothelial Cell Line Increase Cellular ATP Levels. AAPS PharmSciTech. 2021;22:18.
[33] Kanada M, Kim BD, Hardy JW, Ronald JA, Bachmann MH, Bernard MP, et al. Microvesicle-Mediated Delivery of Minicircle DNA Results in Effective Gene-Directed Enzyme Prodrug Cancer Therapy. Mol Cancer Ther. 2019;18:2331-42.
[34] Phinney DG, Di Giuseppe M, Njah J, Sala E, Shiva S, St Croix CM, et al. Mesenchymal stem cells use extracellular vesicles to outsource mitophagy and shuttle microRNAs. Nature Communications. 2015;6:8472.
[35] Hough KP, Trevor JL, Strenkowski JG, Wang Y, Chacko BK, Tousif S, et al. Exosomal transfer of mitochondria from airway myeloid-derived regulatory cells to T cells. Redox Biol. 2018;18:54-64.
[36] Islam MN, Das SR, Emin MT, Wei M, Sun L, Westphalen K, et al. Mitochondrial transfer from bone-marrow-derived stromal cells to pulmonary alveoli protects against acute lung injury. Nat Med. 2012;18:759-65.
[37] Théry C, Witwer KW, Aikawa E, Alcaraz MJ, Anderson JD, Andriantsitohaina R, et al. Minimal information for studies of extracellular vesicles 2018 (MISEV2018): a position statement of the International Society for Extracellular Vesicles and update of the MISEV2014 guidelines. Journal of Extracellular Vesicles. 2018;7:1535750.
[38] Dave KM, Han L, Jackson MA, Kadlecik L, Duvall CL, D SM. DNA Polyplexes of a Phosphorylcholine-Based Zwitterionic Polymer for Gene Delivery. Pharm Res. 2020;37:176.
[39] Braganza A, Li J, Zeng X, Yates NA, Dey NB, Andrews J, et al. UBE3B Is a Calmodulin-regulated, Mitochondrion-associated E3 Ubiquitin Ligase. J Biol Chem. 2017;292:2470-84.
[40] Perkins DN, Pappin DJ, Creasy DM, Cottrell JS. Probability-based protein identification by searching sequence databases using mass spectrometry data. Electrophoresis. 1999;20:3551-67.
[41] Orfila JE, Dietz RM, Rodgers KM, Dingman A, Patsos OP, Cruz-Torres I, et al. Experimental pediatric stroke shows age-specific recovery of cognition and role of hippocampal Nogo-A receptor signaling. J Cereb Blood Flow Metab. 2020;40:588-99.
[42] Herson PS, Bombardier CG, Parker SM, Shimizu T, Klawitter J, Klawitter J, et al. Experimental pediatric arterial ischemic stroke model reveals sex-specific estrogen signaling. Stroke. 2013;44:759-63.

[43] Orfila JE, Grewal H, Dietz RM, Strnad F, Shimizu T, Moreno M, et al. Delayed inhibition of tonic inhibition enhances functional recovery following experimental ischemic stroke. J Cereb Blood Flow Metab. 2019;39:1005-14.
[44] Dai X, Chen J, Xu F, Zhao J, Cai W, Sun Z, et al. TGFα preserves oligodendrocyte lineage cells and improves white matter integrity after cerebral ischemia. J Cereb Blood Flow Metab. 2020;40:639-55.
[45] György B, Hung ME, Breakefield XO, Leonard JN. Therapeutic applications of extracellular vesicles: clinical promise and open questions. Annu Rev Pharmacol Toxicol. 2015;55:439-64.
[46] Ferguson SW, Nguyen J. Exosomes as therapeutics: The implications of molecular composition and exosomal heterogeneity. J Control Release. 2016;228:179-90.
[47] Balaj L, Lessard R, Dai L, Cho Y-J, Pomeroy SL, Breakefield XO, et al. Tumour microvesicles contain retrotransposon elements and amplified oncogene sequences. Nat Commun. 2011;2:180-.
[48] Cai J, Han Y, Ren H, Chen C, He D, Zhou L, et al. Extracellular vesicle-mediated transfer of donor genomic DNA to recipient cells is a novel mechanism for genetic influence between cells. J Mol Cell Biol. 2013;5:227-38.
[49] Thakur BK, Zhang H, Becker A, Matei I, Huang Y, Costa-Silva B, et al. Double-stranded DNA in exosomes: a novel biomarker in cancer detection. Cell Res. 2014;24:766-9.
[50] Oldendorf WH, Cornford ME, Brown WJ. The large apparent work capability of the blood-brain barrier: a study of the mitochondrial content of capillary endothelial cells in brain and other tissues of the rat. Ann Neurol. 1977;1:409-17.
[51] Parodi-Rullán R, Sone JY, Fossati S. Endothelial Mitochondrial Dysfunction in Cerebral Amyloid Angiopathy and Alzheimer's Disease. J Alzheimers Dis. 2019;72:1019-39.
[52] Meckes DG, Jr., Raab-Traub N. Microvesicles and viral infection. J Virol. 2011;85:12844-54.
[53] Antonyak MA, Cerione RA. Emerging picture of the distinct traits and functions of microvesicles and exosomes. Proceedings of the National Academy of Sciences. 2015;112:3589.
[54] Haney MJ, Klyachko NL, Zhao Y, Gupta R, Plotnikova EG, He Z, et al. Exosomes as drug delivery vehicles for Parkinson's disease therapy. Journal of controlled release : official journal of the Controlled Release Society. 2015;207:18-30.
[55] Midekessa G, Godakumara K, Ord J, Viil J, Lättekivi F, Dissanayake K, et al. Zeta Potential of Extracellular Vesicles: Toward Understanding the Attributes that Determine Colloidal Stability. ACS Omega. 2020;5:16701-10.
[56] Matsumoto A, Takahashi Y, Nishikawa M, Sano K, Morishita M, Charoenviriyakul C, et al. Role of Phosphatidylserine-Derived Negative Surface Charges in the Recognition and Uptake of Intravenously Injected B16BL6-Derived Exosomes by Macrophages. Journal of Pharmaceutical Sciences. 2017;106:168-75.
[57] Riches A, Campbell E, Borger E, Powis S. Regulation of exosome release from mammary epithelial and breast cancer cells – A new regulatory pathway. European Journal of Cancer. 2014;50:1025-34.
[58] dos Santos T, Varela J, Lynch I, Salvati A, Dawson KA. Quantitative Assessment of the Comparative Nanoparticle-Uptake Efficiency of a Range of Cell Lines. Small. 2011;7:3341-9.
[59] Théry C, Ostrowski M, Segura E. Membrane vesicles as conveyors of immune responses. Nature Reviews Immunology. 2009;9:581-93.

[60] Muralidharan-Chari V, Clancy JW, Sedgwick A, Souza-Schorey C. Microvesicles: mediators of extracellular communication during cancer progression. Journal of Cell Science. 2010;123:1603.
[61] Gray WD, Mitchell AJ, Searles CD. An accurate, precise method for general labeling of extracellular vesicles. MethodsX. 2015;2:360-7.
[62] Kong F, Zhang L, Wang H, Yuan G, Guo A, Li Q, et al. Impact of collection, isolation and storage methodology of circulating microvesicles on flow cytometric analysis. Exp Ther Med. 2015;10:2093-101.
[63] Chuo ST-Y, Chien JC-Y, Lai CP-K. Imaging extracellular vesicles: current and emerging methods. J Biomed Sci. 2018;25:91-.
[64] Lucchetti D, Battaglia A, Ricciardi-Tenore C, Colella F, Perelli L, De Maria R, et al. Measuring Extracellular Vesicles by Conventional Flow Cytometry: Dream or Reality? Int J Mol Sci. 2020;21.
[65] Jeyaram A, Jay SM. Preservation and Storage Stability of Extracellular Vesicles for Therapeutic Applications. AAPS J. 2017;20:1-.
[66] Lőrincz ÁM, Timár CI, Marosvári KA, Veres DS, Otrokocsi L, Kittel Á, et al. Effect of storage on physical and functional properties of extracellular vesicles derived from neutrophilic granulocytes. Journal of extracellular vesicles. 2014;3:25465-.
[67] Shtam TA, Kovalev RA, Varfolomeeva EY, Makarov EM, Kil YV, Filatov MV. Exosomes are natural carriers of exogenous siRNA to human cells in vitro. Cell Communication and Signaling. 2013;11:88.
[68] Kooijmans SAA, Stremersch S, Braeckmans K, de Smedt SC, Hendrix A, Wood MJA, et al. Electroporation-induced siRNA precipitation obscures the efficiency of siRNA loading into extracellular vesicles. Journal of Controlled Release. 2013;172:229-38.
[69] Morishita M, Takahashi Y, Matsumoto A, Nishikawa M, Takakura Y. Exosome-based tumor antigens-adjuvant co-delivery utilizing genetically engineered tumor cell-derived exosomes with immunostimulatory CpG DNA. Biomaterials. 2016;111:55-65.
[70] Suh W, Han S-O, Yu L, Kim SW. An Angiogenic, Endothelial-Cell-Targeted Polymeric Gene Carrier. Molecular Therapy. 2002;6:664-72.
[71] Tanner FC, Carr DP, Nabel GJ, Nabel EG. Transfection of human endothelial cells. Cardiovascular Research. 1997;35:522-8.
[72] Cufaro MC, Pieragostino D, Lanuti P, Rossi C, Cicalini I, Federici L, et al. Extracellular Vesicles and Their Potential Use in Monitoring Cancer Progression and Therapy: The Contribution of Proteomics. J Oncol. 2019;2019:1639854-.
[73] György B, Szabó TG, Pásztói M, Pál Z, Misják P, Aradi B, et al. Membrane vesicles, current state-of-the-art: emerging role of extracellular vesicles. Cell Mol Life Sci. 2011;68:2667-88.
[74] Intra J, Salem AK. Characterization of the transgene expression generated by branched and linear polyethylenimine-plasmid DNA nanoparticles in vitro and after intraperitoneal injection in vivo. J Control Release. 2008;130:129-38.
[75] Soundara Manickam D, Oupicky D. Polyplex gene delivery modulated by redox potential gradients. J Drug Target. 2006;14:519-26.
[76] Zhu JY, Zheng DW, Zhang MK, Yu WY, Qiu WX, Hu JJ, et al. Preferential Cancer Cell Self-Recognition and Tumor Self-Targeting by Coating Nanoparticles with Homotypic Cancer Cell Membranes. Nano Lett. 2016;16:5895-901.
[77] Jones CH, Chen C-K, Ravikrishnan A, Rane S, Pfeifer BA. Overcoming nonviral gene delivery barriers: perspective and future. Mol Pharm. 2013;10:4082-98.

[78] Tseng WC, Haselton FR, Giorgio TD. Mitosis enhances transgene expression of plasmid delivered by cationic liposomes. Biochim Biophys Acta. 1999;1445:53-64.
[79] Vaughan EE, DeGiulio JV, Dean DA. Intracellular trafficking of plasmids for gene therapy: mechanisms of cytoplasmic movement and nuclear import. Curr Gene Ther. 2006;6:671-81.
[80] Poller B, Gutmann H, Krahenbuhl S, Weksler B, Romero I, Couraud PO, et al. The human brain endothelial cell line hCMEC/D3 as a human blood-brain barrier model for drug transport studies. J Neurochem. 2008;107:1358-68.
[81] Cai HQ, Catts VS, Webster MJ, Galletly C, Liu D, O'Donnell M, et al. Increased macrophages and changed brain endothelial cell gene expression in the frontal cortex of people with schizophrenia displaying inflammation. Mol Psychiatry. 2020;25:761-75.
[82] Yuan D, Zhao Y, Banks WA, Bullock KM, Haney M, Batrakova E, et al. Macrophage exosomes as natural nanocarriers for protein delivery to inflamed brain. Biomaterials. 2017;142:1-12.
[83] Bunggulawa EJ, Wang W, Yin T, Wang N, Durkan C, Wang Y, et al. Recent advancements in the use of exosomes as drug delivery systems. J Nanobiotechnology. 2018;16:81-.
[84] Haqqani AS, Delaney CE, Tremblay T-L, Sodja C, Sandhu JK, Stanimirovic DB. Method for isolation and molecular characterization of extracellular microvesicles released from brain endothelial cells. Fluids and Barriers of the CNS. 2013;10:4.
[85] van den Boorn JG, Schlee M, Coch C, Hartmann G. SiRNA delivery with exosome nanoparticles. Nat Biotechnol. 2011;29:325-6.
[86] Stegmann T, Legendre JY. Gene transfer mediated by cationic lipids: lack of a correlation between lipid mixing and transfection. Biochim Biophys Acta. 1997;1325:71-9.
[87] Pisitkun T, Shen R-F, Knepper MA. Identification and proteomic profiling of exosomes in human urine. Proceedings of the National Academy of Sciences of the United States of America. 2004;101:13368.
[88] Valadi H, Ekström K, Bossios A, Sjöstrand M, Lee JJ, Lötvall JO. Exosome-mediated transfer of mRNAs and microRNAs is a novel mechanism of genetic exchange between cells. Nat Cell Biol. 2007;9:654-9.
[89] Badding MA, Lapek JD, Friedman AE, Dean DA. Proteomic and functional analyses of protein-DNA complexes during gene transfer. Mol Ther. 2013;21:775-85.
[90] Bai H, Lester GMS, Petishnok LC, Dean DA. Cytoplasmic transport and nuclear import of plasmid DNA. Biosci Rep. 2017;37:BSR20160616.
[91] Mulcahy LA, Pink RC, Carter DR. Routes and mechanisms of extracellular vesicle uptake. J Extracell Vesicles. 2014;3.
[92] Al-Nedawi K, Meehan B, Micallef J, Lhotak V, May L, Guha A, et al. Intercellular transfer of the oncogenic receptor EGFRvIII by microvesicles derived from tumour cells. Nat Cell Biol. 2008;10:619-24.
[93] Mathivanan S, Simpson RJ. ExoCarta: A compendium of exosomal proteins and RNA. PROTEOMICS. 2009;9:4997-5000.
[94] Dozio V, Sanchez JC. Characterisation of extracellular vesicle-subsets derived from brain endothelial cells and analysis of their protein cargo modulation after TNF exposure. J Extracell Vesicles. 2017;6:1302705.
[95] Bruschi M, Santucci L, Ravera S, Bartolucci M, Petretto A, Calzia D, et al. Metabolic Signature of Microvesicles from Umbilical Cord Mesenchymal Stem Cells of Preterm and Term Infants. Proteomics Clin Appl. 2018;12:e1700082.

[96] Sansone P, Savini C, Kurelac I, Chang Q, Amato LB, Strillacci A, et al. Packaging and transfer of mitochondrial DNA via exosomes regulate escape from dormancy in hormonal therapy-resistant breast cancer. Proceedings of the National Academy of Sciences. 2017;114:E9066.
[97] Picca A, Guerra F, Calvani R, Marini F, Biancolillo A, Landi G, et al. Mitochondrial Signatures in Circulating Extracellular Vesicles of Older Adults with Parkinson's Disease: Results from the EXosomes in PArkiNson's Disease (EXPAND) Study. J Clin Med. 2020;9:504.
[98] Jiang D, Gao F, Zhang Y, Wong DSH, Li Q, Tse H-F, et al. Mitochondrial transfer of mesenchymal stem cells effectively protects corneal epithelial cells from mitochondrial damage. Cell Death Dis. 2016;7:e2467-e.
[99] Gebara N, Rossi A, Skovronova R, Aziz JM, Asthana A, Bussolati B. Extracellular Vesicles, Apoptotic Bodies and Mitochondria: Stem Cell Bioproducts for Organ Regeneration. Current Transplantation Reports. 2020;7:105-13.
[100] Sinclair KA, Yerkovich ST, Hopkins PM-A, Chambers DC. Characterization of intercellular communication and mitochondrial donation by mesenchymal stromal cells derived from the human lung. Stem cell research & therapy. 2016;7:91-.
[101] Nuzzi R, Buono L, Scalabrin S, De Iuliis M, Bussolati B. Effect of Stem Cell-Derived Extracellular Vesicles on Damaged Human Corneal Endothelial Cells. Stem Cells Int. 2021;2021:6644463-.
[102] Samaeekia R, Rabiee B, Putra I, Shen X, Park YJ, Hematti P, et al. Effect of Human Corneal Mesenchymal Stromal Cell-derived Exosomes on Corneal Epithelial Wound Healing. Invest Ophthalmol Vis Sci. 2018;59:5194-200.
[103] Bruno S, Tapparo M, Collino F, Chiabotto G, Deregibus MC, Soares Lindoso R, et al. Renal Regenerative Potential of Different Extracellular Vesicle Populations Derived from Bone Marrow Mesenchymal Stromal Cells. Tissue Eng Part A. 2017;23:1262-73.
[104] Ragni E, Perucca Orfei C, De Luca P, Mondadori C, Viganò M, Colombini A, et al. Inflammatory priming enhances mesenchymal stromal cell secretome potential as a clinical product for regenerative medicine approaches through secreted factors and EV-miRNAs: the example of joint disease. Stem Cell Res Ther. 2020;11:165.
[105] Chaturvedi RK, Beal MF. Mitochondrial approaches for neuroprotection. Ann N Y Acad Sci. 2008;1147:395-412.
[106] Lo EH, Moskowitz MA, Jacobs TP. Exciting, radical, suicidal: how brain cells die after stroke. Stroke. 2005;36:189-92.
[107] Moskowitz MA, Lo EH, Iadecola C. The science of stroke: mechanisms in search of treatments. Neuron. 2010;67:181-98.
[108] Cottet-Rousselle C, Ronot X, Leverve X, Mayol JF. Cytometric assessment of mitochondria using fluorescent probes. Cytometry A. 2011;79:405-25.
[109] Scharping NE, Menk AV, Moreci RS, Whetstone RD, Dadey RE, Watkins SC, et al. The Tumor Microenvironment Represses T Cell Mitochondrial Biogenesis to Drive Intratumoral T Cell Metabolic Insufficiency and Dysfunction. Immunity. 2016;45:374-88.
[110] Anne Stetler R, Leak RK, Gao Y, Chen J. The dynamics of the mitochondrial organelle as a potential therapeutic target. J Cereb Blood Flow Metab. 2013;33:22-32.
[111] Panfoli I, Ravera S, Podestà M, Cossu C, Santucci L, Bartolucci M, et al. Exosomes from human mesenchymal stem cells conduct aerobic metabolism in term and preterm newborn infants. FASEB J. 2016;30:1416-24.

[112] Puhm F, Afonyushkin T, Resch U, Obermayer G, Rohde M, Penz T, et al. Mitochondria Are a Subset of Extracellular Vesicles Released by Activated Monocytes and Induce Type I IFN and TNF Responses in Endothelial Cells. Circulation Research. 2019;125:43-52.
[113] Zhang X, Hubal MJ, Kraus VB. Immune cell extracellular vesicles and their mitochondrial content decline with ageing. Immunity & Ageing. 2020;17:1.
[114] Tseng N, Lambie SC, Huynh CQ, Sanford B, Patel M, Herson PS, et al. Mitochondrial transfer from mesenchymal stem cells improves neuronal metabolism after oxidant injury in vitro: The role of Miro1. J Cereb Blood Flow Metab. 2021;41:761-70.
[115] Wang P, Henning SM, Heber D. Limitations of MTT and MTS-based assays for measurement of antiproliferative activity of green tea polyphenols. PLoS One. 2010;5:e10202.
[116] Petty RD, Sutherland LA, Hunter EM, Cree IA. Comparison of MTT and ATP-based assays for the measurement of viable cell number. J Biolumin Chemilumin. 1995;10:29-34.
[117] Posimo JM, Unnithan AS, Gleixner AM, Choi HJ, Jiang Y, Pulugulla SH, et al. Viability assays for cells in culture. J Vis Exp. 2014:e50645-e.
[118] Wolf T, Baier SR, Zempleni J. The Intestinal Transport of Bovine Milk Exosomes Is Mediated by Endocytosis in Human Colon Carcinoma Caco-2 Cells and Rat Small Intestinal IEC-6 Cells. J Nutr. 2015;145:2201-6.
[119] Hansen MS, Gadegaard ISE, Arnspang EC, Blans K, Nejsum LN, Rasmussen JT. Specific and Non-Invasive Fluorescent Labelling of Extracellular Vesicles for Evaluation of Intracellular Processing by Intestinal Epithelial Cells. Biomedicines. 2020;8.
[120] Joerger-Messerli MS, Oppliger B, Spinelli M, Thomi G, di Salvo I, Schneider P, et al. Extracellular Vesicles Derived from Wharton's Jelly Mesenchymal Stem Cells Prevent and Resolve Programmed Cell Death Mediated by Perinatal Hypoxia-Ischemia in Neuronal Cells. Cell Transplant. 2018;27:168-80.
[121] Otero-Ortega L, Laso-García F, Frutos MCG-d, Diekhorst L, Martínez-Arroyo A, Alonso-López E, et al. Low dose of extracellular vesicles identified that promote recovery after ischemic stroke. Stem Cell Research & Therapy. 2020;11:70.
[122] Jurgielewicz BJ, Yao Y, Stice SL. Kinetics and Specificity of HEK293T Extracellular Vesicle Uptake using Imaging Flow Cytometry. Nanoscale Research Letters. 2020;15:170.
[123] Saari H, Lázaro-Ibáñez E, Viitala T, Vuorimaa-Laukkanen E, Siljander P, Yliperttula M. Microvesicle- and exosome-mediated drug delivery enhances the cytotoxicity of Paclitaxel in autologous prostate cancer cells. Journal of Controlled Release. 2015;220:727-37.
[124] Joshi BS, de Beer MA, Giepmans BNG, Zuhorn IS. Endocytosis of Extracellular Vesicles and Release of Their Cargo from Endosomes. ACS Nano. 2020;14:4444-55.
[125] Morad G, Carman CV, Hagedorn EJ, Perlin JR, Zon LI, Mustafaoglu N, et al. Tumor-Derived Extracellular Vesicles Breach the Intact Blood–Brain Barrier via Transcytosis. ACS Nano. 2019;13:13853-65.
[126] Costa Verdera H, Gitz-Francois JJ, Schiffelers RM, Vader P. Cellular uptake of extracellular vesicles is mediated by clathrin-independent endocytosis and macropinocytosis. Journal of Controlled Release. 2017;266:100-8.
[127] Dirnagl U, Meisel A. Endogenous neuroprotection: mitochondria as gateways to cerebral preconditioning? Neuropharmacology. 2008;55:334-44.
[128] Hayakawa K, Chan SJ, Mandeville ET, Park JH, Bruzzese M, Montaner J, et al. Protective Effects of Endothelial Progenitor Cell-Derived Extracellular Mitochondria in Brain Endothelium. Stem Cells. 2018;36:1404-10.

[129] Guescini M, Guidolin D, Vallorani L, Casadei L, Gioacchini AM, Tibollo P, et al. C2C12 myoblasts release micro-vesicles containing mtDNA and proteins involved in signal transduction. Exp Cell Res. 2010;316:1977-84.
[130] Koulintchenko M, Temperley RJ, Mason PA, Dietrich A, Lightowlers RN. Natural competence of mammalian mitochondria allows the molecular investigation of mitochondrial gene expression. Hum Mol Genet. 2006;15:143-54.
[131] Amiott EA, Jaehning JA. Mitochondrial transcription is regulated via an ATP "sensing" mechanism that couples RNA abundance to respiration. Mol Cell. 2006;22:329-38.
[132] Waldenström A, Gennebäck N, Hellman U, Ronquist G. Cardiomyocyte microvesicles contain DNA/RNA and convey biological messages to target cells. PLoS One. 2012;7:e34653.
[133] Calabria E, Scambi I, Bonafede R, Schiaffino L, Peroni D, Potrich V, et al. ASCs-Exosomes Recover Coupling Efficiency and Mitochondrial Membrane Potential in an in vitro Model of ALS. Front Neurosci. 2019;13:1070.
[134] Arslan F, Lai RC, Smeets MB, Akeroyd L, Choo A, Aguor ENE, et al. Mesenchymal stem cell-derived exosomes increase ATP levels, decrease oxidative stress and activate PI3K/Akt pathway to enhance myocardial viability and prevent adverse remodeling after myocardial ischemia/reperfusion injury. Stem Cell Research. 2013;10:301-12.
[135] Göran Ronquist K. Extracellular vesicles and energy metabolism. Clinica Chimica Acta. 2019;488:116-21.
[136] Goldberg J, Currais A, Prior M, Fischer W, Chiruta C, Ratliff E, et al. The mitochondrial ATP synthase is a shared drug target for aging and dementia. Aging Cell. 2018;17:e12715.
[137] Dieteren CEJ, Gielen SCAM, Nijtmans LGJ, Smeitink JAM, Swarts HG, Brock R, et al. Solute diffusion is hindered in the mitochondrial matrix. Proceedings of the National Academy of Sciences. 2011;108:8657.
[138] Xu M, Bi X, He X, Yu X, Zhao M, Zang W. Inhibition of the mitochondrial unfolded protein response by acetylcholine alleviated hypoxia/reoxygenation-induced apoptosis of endothelial cells. Cell Cycle. 2016;15:1331-43.
[139] Kotwal GJ, Martin MD, Chien S. Significant upregulation of U1 and U4 spliceosomal snRNAs by ATP nanoliposomes explains acceleration of wound healing, due to increased pre-mRNA processing to functional mRNA. Nanomedicine: Nanotechnology, Biology and Medicine. 2018;14:1289-99.
[140] Puisieux F, Fattal E, Lahiani M, Auger J, Jouannet P, Couvreur P, et al. Liposomes, an Interesting Tool to Deliver a Bioenergetic Substrate (ATP), in Vitro and in Vivo Studies. Journal of Drug Targeting. 1994;2:443-8.
[141] Colleoni F, Padmanabhan N, Yung H-W, Watson ED, Cetin I, Tissot van Patot MC, et al. Suppression of mitochondrial electron transport chain function in the hypoxic human placenta: a role for miRNA-210 and protein synthesis inhibition. PLoS One. 2013;8:e55194-e.

Figure legends

Figure 1. Characterization of EVs derived from hCMEC/D3 (D3-EXO and D3-MV) and RAW 264.7 cells (RAW-EXO and RAW-MV). (*a*) Physicochemical characteristics of EVs: Effective particle diameter (D_{eff}), polydispersity index, and zeta potential were measured using

dynamic light scattering (DLS). The samples at a protein concentration of 0.2 – 0.5 mg/mL were resuspended in 1*x* PBS and 10 mM HEPES buffer, pH 7.4 for D_{eff} and zeta potential measurements, respectively. Representative DLS intensity plots of (*b*) D3-EXO (*c*) D3-MV (*d*) RAW-EXO and (*e*) RAW-MV obtained from measurements on a Malvern Nano Zetasizer. The different traces indicate three measurements of the same sample. (*f*) Total EV protein content (per 25 mL of conditioned media) quantified using MicroBCA protein assay. Data are mean ± SD, n = 11, $^{**}p < 0.01$, $^{****}p < 0.0001$, ns: non-significant as determined using one-way ANOVA and Bonferroni's multiple comparisons test.

Figure 2. Measurement of DNA content in Luc pDNA-loaded EVs derived from hCMEC/D3 endothelial cells and RAW 264.7 macrophages and their transfection activity in the recipient hCMEC/D3 endothelial cells. hCMEC/D3 endothelial and RAW 264.7 macrophages were transfected with Lipofectamine-Luc pDNA at a pDNA dose of 0.5 μg/ or 1.0 μg/well in a 24–well-plate (n = 3). (*a*) The exogenous Luc-DNA content in the isolated EVs were measured by Quant-iT Picogreen dsDNA assay using *Equation 1* and percent DNA loading in EVs is shown in (*b*). Data are presented as mean ± SD (n = 3), $^{*}p < 0.05$, $^{**}p < 0.01$ $^{***}p < 0.001$ by two-way ANOVA of the indicated groups and Bonferroni's multiple comparisons tests. (*c*) Transfection of D3-derived Luc EVs and (*d*) RAW-derived Luc-EVs into the recipient hCMEC/D3 endothelial cells at a DNA dose of 10 ng of DNA/well (n = 4). Luciferase gene expression was expressed as Relative light units (RLU) normalized to total cellular protein content and further normalized to values from the control, untreated cells. Data are presented as mean ± SD (n = 4), $^{*}p < 0.05$, $^{**}p < 0.01$, $^{***}p < 0.001$, $^{****}p < 0.0001$ by two-way ANOVA of the indicated groups and Bonferroni's multiple comparisons test (*e*) Transfection of Lipofectamine-Luc pDNA in

hCMEC/D3 endothelial cells at a treatment dose of 10 ng of DNA/well (n = 5). ***$p < 0.001$, by one-way ANOVA of the indicated groups and Bonferroni's multiple comparisons tests.

Figure 3. Transfer of Mitotracker-labelled mitochondria from hCMEC/D3-derived EVs to the recipient hCMEC/D3 endothelial cells. The donor/source hCMEC/D3 endothelial cells were stained with MitoTracker Deep-Red (MitoT) (250 nM for 30 min) to specifically label polarized mitochondria following which the MitoT-EVs were isolated from conditioned media. The recipient hCMEC/D3 endothelial cells were treated with D3-MitoT-EXO and D3-MitoT-MV at the indicated protein doses and observed under an Olympus IX 73 epifluorescent inverted microscope (Olympus, Pittsburgh, PA) under the Cy5 channel settings at 24 h, 48 h and 72 h post-treatment. The presented data are representative images from three independent experiments (n=4 per experiment). Scale bar = 50 μm.

Figure 4. **Uptake of MitoT-EVs by acute brain slices**. Acute cortical and hippocampal slices from mice subjected to sham middle cerebral artery occlusion procedure were left either untreated (control) or incubated in 50 μg/mL of D3-MitoT-EXO or D3-MitoT-MV for 2 h at 37 °C. Slices were fixed, counterstained with Hoechst 33258 (blue), and visualized on a confocal microscope. Intracellular punctate staining within neurons (magenta) was evident in slices from the cortex (*a*) and dentate gyrus region of the hippocampus (*b*) in both the D3-MitoT-EV and D3-MitoT-MV treated conditions with minimal nonspecific staining in the control condition (*a&b*).

Figure 5. Effects of EV exposure on the cell viability of hCMEC/D3 endothelial cells under normoxic and hypoxic (OGD) conditions. (*a*) hCMEC/D3 endothelial cells were treated with

the indicated EV protein content for 72 h. (*b*) hCMEC/D3 endothelial cells were subjected to 4 h of OGD by exposing the cells in a sealed hypoxia chamber (90% N_2, 5% H_2, 5% CO_2) and glucose-free media at 37 °C in a humidified incubator. OGD exposed hCMEC/D3 endothelial cells were treated with the indicated amounts of naïve D3-EVs for 24 h under 21% O_2 in a humidified incubator. Untreated OGD cells were cultured in glucose-free media under 21% O_2 in a humidified incubator. (*c*) OGD-exposed hCMEC/D3 endothelial cells were treated with the indicated amounts of EVs for the indicated periods. Untreated OGD cells were cultured in glucose-free media 4 h post-OGD in a 21% O_2 humidified incubator. Unless indicated otherwise, normoxic cells cultured in complete media under 21% O_2 in a humidified incubator and cells treated with PEI for 4 h were considered as a positive control. In all cases, the effects of treatment were determined using an ATP assay. Data are represented as mean ± SD (n = 4). Statistical comparisons to the normoxic/hypoxic groups were made using one-way ANOVA Bonferroni's multiple comparisons test.

Figure 6. Formation of EV/ATP5A complexes confirmed using native gel electrophoresis. (*a*) Native PAGE analysis of the EV/ATP5A complexes. 0.5 μg of the indicated samples were electrophoresed in a 4-10% of native PAGE gel and the bands were visualized using Bio-safe Coomassie dye. (*b*) Confluent hCMEC/D3 cells (16,000/well) in 96-well plates were exposed to OGD conditions for 4 h following which the media was replaced with 100 μL of the indicated samples. Cells were incubated for 24 h and washed once in 1*x* PBS prior to measuring cellular ATP levels using a Cell Glo luminescence assay. Data represent average ± SD (n=4).

Supplementary Figure 1. Representative phase-contrast images of hCMEC/D3 endothelial cells and RAW 264.7 cells. (*a*) hCMEC/D3 endothelial cells in complete medium (*b*) hCMEC/D3 endothelial cells in conditioned media (*c*) RAW 264.7 cells in complete medium (*d*) RAW 264.7 cells in conditioned media. The phase-contrast images were captured using EVOS FL Imaging System Technologies at 20x magnification, scale bar = 200 µm.

Supplementary Figure 2. Flow cytometry analysis of EVs. (*a*) Side scatter (SSC)/Forward scatter (FSC) dot plots of 0.1, 0.2, and 0.5 µm microbeads obtained from an Attune NxT Acoustic Focusing Cytometer. The EV gate was defined below 0.5 µm; (*b*) SSC/Calcein-AM (BL1) fluorescent profiles of 0.1, 0.2, and 0.5 µm microbeads used to set the EV gate and establish the measurement settings; (*c*) SSC/Calcein-AM scatter plots and (*d*) histogram of fluorescent signals demonstrating separation of the instrument noise and background signals for free calcein-AM solution in 1*x* PBS. EVs were isolated from hCMEC/D3 and RAW 264.7 cell lines and resuspended in 1*x* PBS. Non-stained RAW-MV (*e*), RAW-EXO (*f*), D3-MV (*g*) and D3-EXO (*h*) were used as negative controls to verify the absence of fluorescent signals in the gated area. Scatter plots of calcein-stained RAW-MV (*i*), RAW-EXO (*j*), D3-MV (*k*) and D3-EXO (*l*). Scatter plots of calcein-stained samples treated with Triton X (1 % v/v): (*m*) RAW-MV (*n*) RAW-EXO (*o*) D3-MV and (*p*) D3-EXO. The data shown are representative plots of n=3 samples.

Supplementary Figure 3. Transfer of mitochondria from RAW-MitoT-EXO and RAW-MitoT-MV to the recipient hCMEC/D3 endothelial cells. The donor/source RAW 264.7 macrophages were stained with MitoTracker Deep-Red (MitoT) (250 nM for 30 min) to specifically label polarized mitochondria following which the MitoT-EVs were isolated from

conditioned media. The recipient hCMEC/D3 endothelial cells were treated with RAW-MitoT-EXO and RAW-MitoT-MV at the indicated protein doses and observed under an Olympus IX 73 epifluorescent inverted microscope (Olympus, Pittsburgh, PA) under the Cy5 channel settings at 24 h, 48 h and 72 h post-treatment. The presented data are representative images from three independent experiments (n=3 per experiment). Scale bar = 50 μm.

Supplementary Figure 4. Modelling oxygen-glucose deprivation (OGD)-induced cell death in hCMEC/D3 endothelial cells. Confluent hCMEC/D3 endothelial cells seeded in a 96-well plate were subjected to OGD conditions for the indicated times. OGD was induced by exposing the cells in a sealed hypoxic (90% N_2, 5% H_2, 5% CO_2) chamber and glucose-free media at 37 °C in a humidified incubator. An ATP assay was performed to measure the cell viability post-OGD exposure. The resulting ATP levels were compared to normoxic cells cultured in complete media. Normoxic cells treated with polyethyleneimine (PEI) for 4 h were used as a positive control. Data are represented as mean ± SD (n = 6). **** $p < 0.0001$ Statistical comparisons were made to normoxic cells by one-way ANOVA followed by Bonferroni's multiple comparisons test.

Supplementary Table 1: Proteins identified in isolated EV as enlisted in Vesiclepedia database

Top 100 EV proteins listed in the Vesiclepedia database were downloaded on 02/14/2021.

Vesiclepedia information		**Expression in**	
No.	**Gene Symbol**	**Naïve D3-EV**	**Naïve RAW-EV**
1	**PDCD6IP**	Not detected	Q80Y09_MOUSE Pdcd6ip protein OS=Mus musculus OX=10090 GN=Pdcd6ip PE=2 SV=1
2	**GAPDH**	G3P_HUMAN Glyceraldehyde-3-phosphate dehydrogenase OS=Homo	D2KHZ9_MOUSE Glyceraldehyde-3-phosphate dehydrogenase OS=Mus musculus

Vesiclepedia information		Expression in	
No.	**Gene Symbol**	**Naïve D3-EV**	**Naïve RAW-EV**
		sapiens OX=9606 GN=GAPDH PE=1 SV=3	OX=10090 GN=GAPDH PE=2 SV=1
3	**HSPA8**	Not detected	Q3UBA6_MOUSE Uncharacterized protein OS=Mus musculus OX=10090 GN=Hspa8 PE=2 SV=1
4	**ACTB**	Not detected	B2RRX1_MOUSE Actin, beta OS=Mus musculus OX=10090 GN=Actb PE=2 SV=1
5	**ANXA2**	ANXA2_HUMAN Annexin A2 OS=Homo sapiens OX=9606 GN=ANXA2 PE=1 SV=2	Not detected
6	**CD9**	Not detected	CD9_MOUSE CD9 antigen OS=Mus musculus OX=10090 GN=Cd9 PE=1 SV=2
7	**PKM**	KPYM_HUMAN Pyruvate kinase PKM OS=Homo sapiens OX=9606 GN=PKM PE=1 SV=4	KPYM_MOUSE Pyruvate kinase PKM OS=Mus musculus OX=10090 GN=Pkm PE=1 SV=4
8	**HSP90AA1**	HS90A_HUMAN Isoform 2 of Heat shock protein HSP 90-alpha OS=Homo sapiens OX=9606 GN=HSP90AA1	Not detected
9	**ENO1**	ENOA_HUMAN Alpha-enolase OS=Homo sapiens OX=9606 GN=ENO1 PE=1 SV=2	ENOA_MOUSE Alpha-enolase OS=Mus musculus OX=10090 GN=Eno1 PE=1 SV=3
10	**ANXA5**	Not detected	ANXA5_MOUSE Annexin A5 OS=Mus musculus OX=10090 GN=Anxa5 PE=1 SV=1
11	**HSP90AB1**	Not detected	1) ENPL_MOUSE Endoplasmin OS=Mus musculus OX=10090 GN=Hsp90b1 PE=1 SV=2 2) HS90B_MOUSE Heat shock protein HSP 90-beta OS=Mus musculus OX=10090 GN=Hsp90ab1 PE=1 SV=3
12	**CD63**	Not detected	Not detected

Vesiclepedia information		Expression in	
No.	**Gene Symbol**	**Naïve D3-EV**	**Naïve RAW-EV**
13	**YWHAZ**	1433Z_HUMAN 14-3-3 protein zeta/delta OS=Homo sapiens OX=9606 GN=YWHAZ PE=1 SV=1	Not detected
14	**YWHAE**	1433E_HUMAN 14-3-3 protein epsilon OS=Homo sapiens OX=9606 GN=YWHAE PE=1 SV=1	Not detected
15	**EEF1A1**	Not detected	EF1A1_MOUSE Elongation factor 1-alpha 1 OS=Mus musculus OX=10090 GN=Eef1a1 PE=1 SV=3
16	**PGK1**	Not detected	PGK1_MOUSE Phosphoglycerate kinase 1 OS=Mus musculus OX=10090 GN=Pgk1 PE=1 SV=4
17	**CLTC**	CLH1_HUMAN Clathrin heavy chain 1 OS=Homo sapiens OX=9606 GN=CLTC PE=1 SV=5	Q5SXR6_MOUSE Clathrin heavy chain OS=Mus musculus OX=10090 GN=Cltc PE=1 SV=1
18	**PPIA**	Not detected	PPIA_MOUSE Peptidyl-prolyl cis-trans isomerase A OS=Mus musculus OX=10090 GN=Ppia PE=1 SV=2
19	**SDCBP**	Not detected	Not detected
20	**ALDOA**	ALDOA_HUMAN Fructose-bisphosphate aldolase A OS=Homo sapiens OX=9606 GN=ALDOA PE=1 SV=2	A6ZI44_MOUSE Fructose-bisphosphate aldolase OS=Mus musculus OX=10090 GN=Aldoa PE=1 SV=1
21	**EEF2**	Not detected	EF2_MOUSE Elongation factor 2 OS=Mus musculus OX=10090 GN=Eef2 PE=1 SV=2
22	**ALB**	ALBU_HUMAN Serum albumin OS=Homo sapiens OX=9606 GN=ALB PE=1 SV=2	ALBU_MOUSE Serum albumin OS=Mus musculus OX=10090 GN=Alb PE=1 SV=3
23	**TPI1**	TPIS_HUMAN Isoform 2 of Triosephosphate isomerase OS=Homo sapiens OX=9606 GN=TPI1	TPIS_MOUSE Triosephosphate isomerase OS=Mus musculus OX=10090 GN=Tpi1 PE=1 SV=4

Vesiclepedia information		Expression in	
No.	**Gene Symbol**	**Naïve D3-EV**	**Naïve RAW-EV**
24	**VCP**	Not detected	TERA_MOUSE Transitional endoplasmic reticulum ATPase OS=Mus musculus OX=10090 GN=Vcp PE=1 SV=4
25	**CFL1**	Not detected	COF1_MOUSE Cofilin-1 OS=Mus musculus OX=10090 GN=Cfl1 PE=1 SV=3
26	**MSN**	Not detected	MOES_MOUSE Moesin OS=Mus musculus OX=10090 GN=Msn PE=1 SV=3
27	**ATP1A1**	Not detected	AT1A1_MOUSE Sodium/potassium-transporting ATPase subunit alpha-1 OS=Mus musculus OX=10090 GN=Atp1a1 PE=1 SV=1
28	**PRDX1**	Not detected	Not detected
29	**MYH9**	MYH9_HUMAN Myosin-9 OS=Homo sapiens OX=9606 GN=MYH9 PE=1 SV=4	MYH9_MOUSE Myosin-9 OS=Mus musculus OX=10090 GN=Myh9 PE=1 SV=4
30	**EZR**	Not detected	Not detected
31	**CD81**	Not detected	Not detected
32	**ANXA6**	Not detected	Not detected
33	**FLOT1**	Not detected	Not detected
34	**YWHAB**	Not detected	Not detected
35	**LDHB**	Not detected	Not detected
36	**SLC3A2**	4F2_HUMAN 4F2 cell-surface antigen heavy chain OS=Homo sapiens OX=9606 GN=SLC3A2 PE=1 SV=3	4F2_MOUSE 4F2 cell-surface antigen heavy chain OS=Mus musculus OX=10090 GN=Slc3a2 PE=1 SV=1
37	**GNB1**	Not detected	
38	**PFN1**	Not detected	PROF1_MOUSE Profilin-1 OS=Mus musculus OX=10090 GN=Pfn1 PE=1 SV=2
39	**TSG101**	Not detected	Not detected
40	**YWHAQ**	1433T_HUMAN 14-3-3 protein theta OS=Homo sapiens OX=9606 GN=YWHAQ PE=1 SV=1	Not detected
41	**GNAI2**	Not detected	Not detected

Vesiclepedia information		Expression in	
No.	**Gene Symbol**	**Naïve D3-EV**	**Naïve RAW-EV**
42	**CLIC1**	Not detected	Q542F1_MOUSE Chloride intracellular channel protein OS=Mus musculus OX=10090 GN=Clic1 PE=1 SV=1
43	**ANXA1**	ANXA1_HUMAN Annexin A1 OS=Homo sapiens OX=9606 GN=ANXA1 PE=1 SV=2	Not detected
44	**ITGB1**	Not detected	1) ITB2_MOUSE Integrin beta-2 OS=Mus musculus OX=10090 GN=Itgb2 PE=1 SV=2 2) ITB1_MOUSE Integrin beta-1 OS=Mus musculus OX=10090 GN=Itgb1 PE=1 SV=1
45	**LDHA**	LDHA_HUMAN Isoform 3 of L-lactate dehydrogenase A chain OS=Homo sapiens OX=9606 GN=LDHA	A0A1B0GSR9_MOUSE L-lactate dehydrogenase OS=Mus musculus OX=10090 GN=Ldha PE=1 SV=1
46	**FASN**	FAS_HUMAN Fatty acid synthase OS=Homo sapiens OX=9606 GN=FASN PE=1 SV=3	FAS_MOUSE Fatty acid synthase OS=Mus musculus OX=10090 GN=Fasn PE=1 SV=2
47	**CDC42**	Not detected	Not detected
48	**RAP1B**	Not detected	Not detected
49	**CCT2**	TCPB_HUMAN T-complex protein 1 subunit beta OS=Homo sapiens OX=9606 GN=CCT2 PE=1 SV=4	TCPB_MOUSE T-complex protein 1 subunit beta OS=Mus musculus OX=10090 GN=Cct2 PE=1 SV=4
50	**YWHAG**	1433G_HUMAN 14-3-3 protein gamma OS=Homo sapiens OX=9606 GN=YWHAG PE=1 SV=2	Not detected
51	**GNB2**	Not detected	Not detected
52	**ACTN4**	ACTN4_HUMAN Alpha-actinin-4 OS=Homo sapiens OX=9606 GN=ACTN4 PE=1 SV=2	Not detected
53	**RAB5C**	Not detected	RAB5C_MOUSE Ras-related protein Rab-5C OS=Mus musculus OX=10090 GN=Rab5c PE=1 SV=2

Vesiclepedia information		Expression in	
No.	**Gene Symbol**	**Naïve D3-EV**	**Naïve RAW-EV**
54	**C3**	Not detected	Not detected
55	**RAB10**	Not detected	Not detected
56	**HIST1H4A**	H4_HUMAN Histone H4 OS=Homo sapiens OX=9606 GN=HIST1H4A PE=1 SV=2	Not detected
57	**KRT1**	1) K2C1_HUMAN Keratin, type II cytoskeletal 1 OS=Homo sapiens OX=9606 GN=KRT1 PE=1 SV=6 2) K1C9_HUMAN Keratin, type I cytoskeletal 9 OS=Homo sapiens OX=9606 GN=KRT9 PE=1 SV=3 3) K1C10_HUMAN Keratin, type I cytoskeletal 10 OS=Homo sapiens OX=9606 GN=KRT10 PE=1	E9Q1Z0_MOUSE Keratin 90 OS=Mus musculus OX=10090 GN=Krt90 PE=1 SV=1
58	**FN1**	FINC_HUMAN Fibronectin OS=Homo sapiens OX=9606 GN=FN1 PE=1 SV=4	Not detected
59	**AHCY**	SAHH_HUMAN Adenosylhomocysteinase OS=Homo sapiens OX=9606 GN=AHCY PE=1 SV=4	Not detected
60	**A2M**	Not detected	Not detected
61	**BSG**	Not detected	Not detected
62	**ACTN1**	ACTN1_HUMAN Isoform 3 of Alpha-actinin-1 OS=Homo sapiens OX=9606 GN=ACTN1	Not detected
63	**ANXA7**	Not detected	Not detected
64	**ACLY**	ACLY_HUMAN ATP-citrate synthase OS=Homo sapiens OX=9606 GN=ACLY PE=1 SV=3	Not detected
65	**HIST1H4B**	Not detected	Not detected
66	**GDI2**	Not detected	Q3TIY6_MOUSE Rab GDP dissociation inhibitor OS=Mus

Vesiclepedia information		Expression in	
No.	**Gene Symbol**	**Naïve D3-EV**	**Naïve RAW-EV**
			musculus OX=10090 GN=Gdi2 PE=2 SV=1
67	**FLNA**	FLNA_HUMAN Filamin-A OS=Homo sapiens OX=9606 GN=FLNA PE=1 SV=4	Not detected
68	**UBA1**	Not detected	A0A1S6GWH5_MOUSE Uncharacterized protein OS=Mus musculus OX=10090 GN=Uba1 PE=2 SV=1
69	**GNAS**	Not detected	Not detected
70	**GSN**	Not detected	Not detected
71	**CCT4**	TCPD_HUMAN T-complex protein 1 subunit delta OS=Homo sapiens OX=9606 GN=CCT4 PE=1 SV=4	TCPD_MOUSE T-complex protein 1 subunit delta OS=Mus musculus OX=10090 GN=Cct4 PE=1 SV=3
72	**RAN**	Not detected	Not detected
73	**PRDX2**	Not detected	Not detected
74	**RHOA**	Not detected	Not detected
75	**CCT3**	Not detected	TCPG_MOUSE T-complex protein 1 subunit gamma OS=Mus musculus OX=10090 GN=Cct3 PE=1 SV=1
76	**RAC1**	Not detected	Not detected
77	**LGALS3BP**	LG3BP_HUMAN Galectin-3-binding protein OS=Homo sapiens OX=9606 GN=LGALS3BP PE=1 SV=1	LG3BP_MOUSE Galectin-3-binding protein OS=Mus musculus OX=10090 GN=Lgals3bp PE=1 SV=1
78	**TCP1**	Not detected	TCPA_MOUSE T-complex protein 1 subunit alpha OS=Mus musculus OX=10090 GN=Tcp1 PE=1 SV=3
79	**KRT10**	Not detected	
80	**CAP1**	Not detected	CAP1_MOUSE Adenylyl cyclase-associated protein 1 OS=Mus musculus OX=10090 GN=Cap1 PE=1 SV=4
81	**RAB7A**	Not detected	Not detected

Vesiclepedia information		Expression in	
No.	**Gene Symbol**	**Naïve D3-EV**	**Naïve RAW-EV**
82	**TUBB4B**	1) TBB5_HUMAN Tubulin beta chain OS=Homo sapiens OX=9606 GN=TUBB PE=1 SV=2 2) TBB4B_HUMAN Tubulin beta-4B chain OS=Homo sapiens OX=9606 GN=TUBB4B PE=1 SV=1	Not detected
83	**HSPA5**	Not detected	BIP_MOUSE Endoplasmic reticulum chaperone BiP OS=Mus musculus OX=10090 GN=Hspa5 PE=1 SV=3
84	**IQGAP1**	Not detected	Not detected
85	**GPI**	Not detected	Not detected
86	**RALA**	Not detected	Not detected
87	**KPNB1**	IMB1_HUMAN Importin subunit beta-1 OS=Homo sapiens OX=9606 GN=KPNB1 PE=1 SV=2	Not detected
88	**HIST1H4I**	Not detected	Not detected
89	**TFRC**	Not detected	Not detected
90	**EIF4A1**	1) EIF3L_HUMAN Eukaryotic translation initiation factor 3 subunit L OS=Homo sapiens OX=9606 GN=EIF3L PE=1 SV=1 2) DDX17_HUMAN Probable ATP-dependent RNA helicase DDX17 OS=Homo sapiens OX=9606 GN=DDX17 PE=1 SV=2	1) B7ZWF1_MOUSE Ddx3x protein OS=Mus musculus OX=10090 GN=Ddx3x PE=2 SV=1 2) IF4A3_MOUSE Eukaryotic initiation factor 4A-III OS=Mus musculus OX=10090 GN=Eif4a3 PE=1 SV=3 3) Q8VH52_MOUSE Translation initiation factor-3 subunit 5 (Fragment) OS=Mus musculus OX=10090 GN=Eif3f PE=2 SV=1
91	**HIST4H4**	Not detected	Not detected
92	**CCT8**	TCPQ_HUMAN T-complex protein 1 subunit theta OS=Homo sapiens OX=9606 GN=CCT8 PE=1 SV=4	Q8BVY8_MOUSE Uncharacterized protein OS=Mus musculus OX=10090 GN=Cct8 PE=2 SV=1

Vesiclepedia information		Expression in	
No.	**Gene Symbol**	**Naïve D3-EV**	**Naïve RAW-EV**
93	**TLN1**	Not detected	Q80TM2_MOUSE MKIAA1027 protein (Fragment) OS=Mus musculus OX=10090 GN=Tln1 PE=2 SV=4
94	**HIST1H4K**	Not detected	Not detected
95	**HIST1H4H**	Not detected	Not detected
96	**CCT6A**	TCPZ_HUMAN T-complex protein 1 subunit zeta OS=Homo sapiens OX=9606 GN=CCT6A PE=1 SV=3	Not detected
97	**ANXA11**	Not detected	Not detected
98	**HIST1H4J**	Not detected	Not detected
99	**HIST1H4F**	Not detected	Not detected
100	**HIST1H4D**	Not detected	Not detected